NBP 13-10

Phantastic cruise report

Contents

1. Introduction and overview

Anne-Carlijn Alderkamp – Chief Scientist

The NBP-13-10 cruise was divided in two segments, the first part of the cruise from Punta Arenas to Rothera Station of the British Antarctic Survey, Nov 19 - Dec 3, 2013, was directed by chief scientist Dr. Kathryn Smith whose group disembarked at Rothera. This is the end-of-cruise report of the second part of the cruise from Rothera Station to Hobart, Dec 3, 2013 – 23 Jan, 2014, B-244 (Fig 1.1). The main project on the cruise was the Phantastic project: *Phaeocystis antarctica* adaptive responses in the Antarctic ecosystem with principal investigators Kevin R. Arrigo of Stanford University (NSF grant #1142018) and Anton F. Post of Marine Biological Laboratories (MBL, NSF grant #1142095), neither of whom were on board. The main aim of the cruise was to sample phytoplankton populations dominated by the haptophyte *Phaeocystis antarctica* in different Antarctic environments, specifically in the Ross Sea and the Antarctic Circumpolar Current (ACC), to study which factors that control the growth of this phytoplankton. The international science team of 11 researchers from various institutes (see appendix B) collected samples to study the phytoplankton physiology and photosynthetic parameters and their gene expression through transcriptomic analysis. Moreover, we sampled for concentrations of nutrients, trace metals, and components of the sulfur cycle. The main activity on the cruise was sampling the upper 300 m of the water column using both the trace metal clean CTD system and the conventional CTD system. Moreover, to study the responses of phytoplankton to changes in light and iron availability, we performed bioassay incubation experiments at in situ water temperatures in deck incubators. Trace metal clean (TMC) work was done free from contaminations from the ship's environment in the TMC van and a TMC bubble that was built in the wetlab of the "N.B. Palmer". Moreover, we studied phytoplankton productivity using radiolabeled C14 in the Radvan. Finally, we used the underway system of the NB Palmer to sample surface waters and gather sensor data.

Sea ice concentrations and extent were unusually high everywhere in the western Antarctic in the 2013-14 season. This affected our transit in and out of Marguerite Bay to let the Smith group disembark, our traveling distance from Rothera to the Ross Sea as we had to go around the sea ice, and our transit into the Ross Sea. It took 17 days to transit from Rothera to the Ross Sea, leaving only 16 days of research time in the Ross Sea and 8 days in the ACC. Moreover, more icebreaking and a longer transit route in combination with a long cruise resulted in very limited fuel availability in the Ross Sea to ensure enough fuel reserves to reach Hobart. The lack of time and fuel severely limited our cruise track options and the distance we could travel to sample and as a result we did not sample the Terra Nova Bay area. Fortunately, the weather was very good during most of our sampling, which allowed for an efficient use of the limited time available.

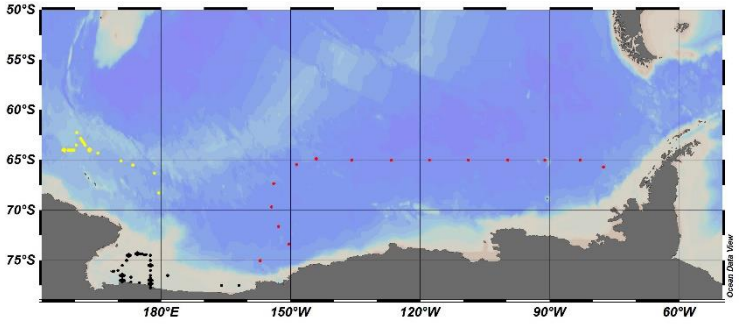

Figure 1.1. Stations sampled during the NBP 13-10 "Phantastic" cruise. Red stations (Sta 1-15) are part of the Rothera to Ross Sea (RotR) transect, black stations (Sta 16-114) are in the Ross Sea, yellow stations (Sta 115-152) are in or near the Antarctic Circumpolar Current (ACC).

We sampled a total of 152 stations (See appendix A) that can be divided into three different areas, Rothera to Ross Sea (RothR), Ross Sea, and in or near the ACC (Fig 1.1). Moreover, in the Ross Sea we performed four bioassay experiments with manipulations of iron and light

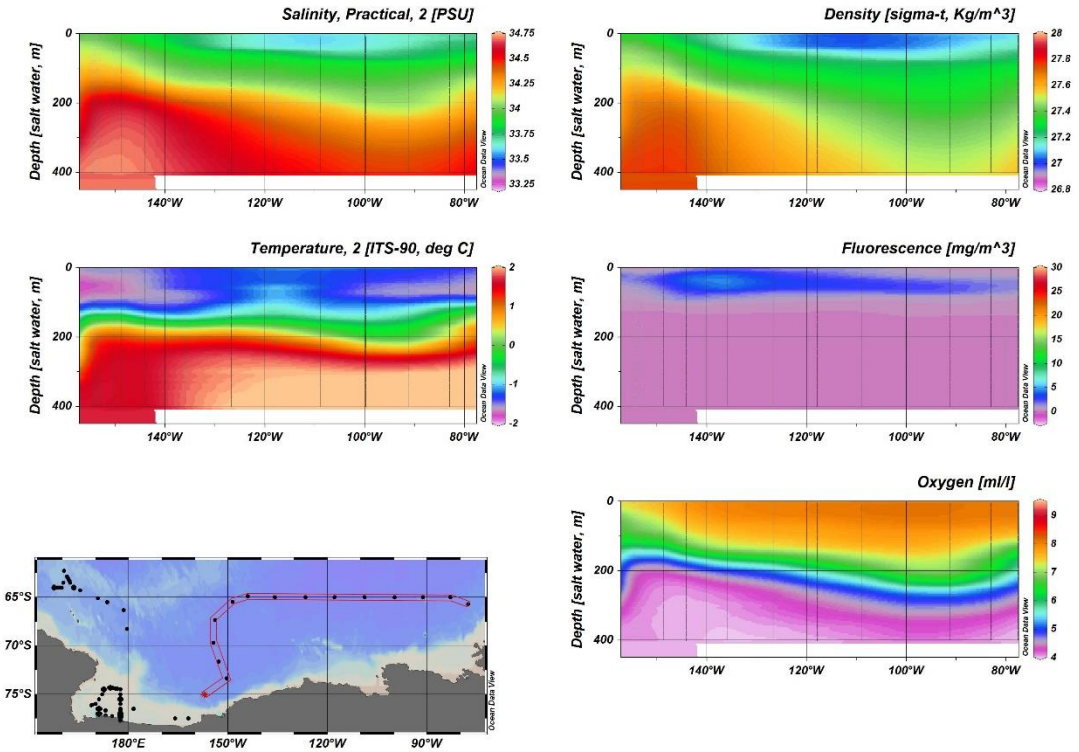

Figure 1.2. Section plots of Rothera to Ross Sea (Roth) transect. Salinity, Temperature, Density (σ_t), Fluorescence and Oxygen data from the CTD sensors are plotted versus longitude.

conditions to study the responses of phytoplankton to different iron and light availability. In the ACC we performed six bioassay experiments where only the iron concentrations were manipulated (see section 3). Finally, we collected samples for several projects not directly related to the Phantastic program, but that provide a suite of data that may be related to the core parameters sampled on both the stations and the bioassay experiments (See sections 10 through 16).

1.1 Rothera to Ross Sea (RothR) transect

The RothR transect (Dec 5- Dec 19) followed 65°S latitude to avoid the sea ice until 150°W, where we headed south, through sea ice to reach the Ross Sea Polynya. The reduced salinity (< 33.8) and low temperature (< -1°C) in surface waters (<100 m) suggest sea ice melt water effects that resulted in a relatively stratified water column (Fig 1.2). In the deeper waters (>200 m depth) of the eastern end of the transect we observed warm water (1.8 °C) that is likely Circumpolar Deep Water (CDW). We found low phytoplankton biomass (< 2 μg L^{-1} Chl *a*) throughout surface waters of the transect, possibly because of the early season and only recent melting of the sea ice. Moreover, DFe concentrations in surface waters were very low and likely limiting phytoplankton growth (see section 6). FlowCAM analysis showed that the phytoplankton populations were mostly dominated by small diatoms (see section 5).

1.2 Ross Sea

The phytoplankton bloom in the Ross Sea showed high biomass in both the central and western polynya (Fig 1.3). We sampled two transects, the first south-to north station (Sta 20-60) followed high phytoplankton biomass in the central polynya, the second north-to south transect (Sta 75-112) high biomass in the western polynya.

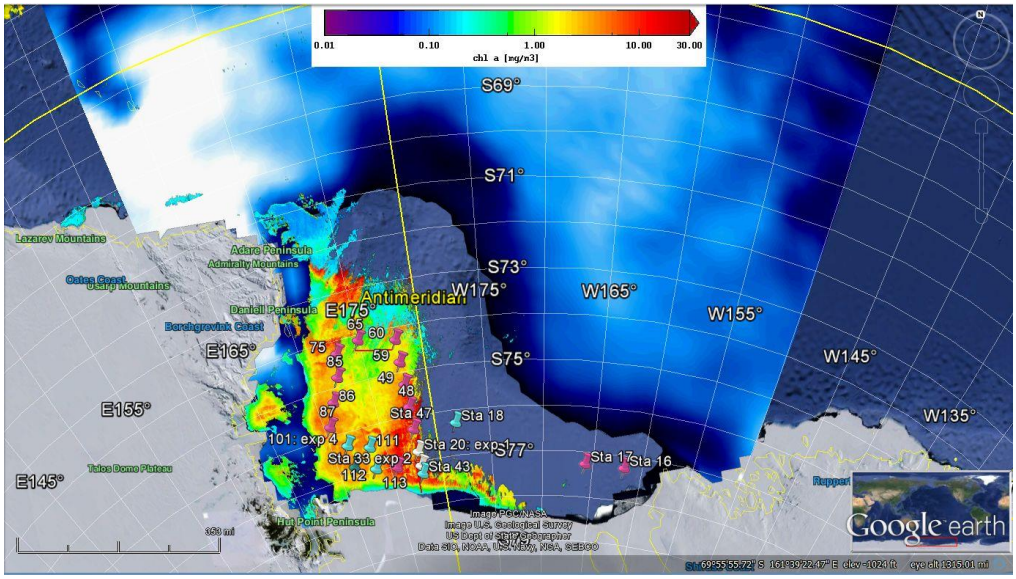

Figure 1.3. Ross Sea stations plotted using Google Earth with chlorophyll *a* and sea ice concentrations derived from satellite data. We sampled two transects, the first south-to north station (Sta 20-60) followed high phytoplankton biomass in the central polynya, the second north-to south transect (Sta 75-112) followed high biomass in the western polynya. Purple stations were dominated by diatoms, white stations by *Phaeocystis antarctica* and blue stations had a mixed phytoplankton population.

The section plots of the south-to-north transect in the central polynya (Fig 1.4) show relatively high salinity throughout the water column. The elevated temperature at the surface (<50 m depth) suggest some solar warming of surface waters, resulting in weak stratification of the upper water column. In the western transect salinity in surface waters was lower than in the central polynya transect (Fig 1.5) suggesting sea ice melt water input, especially in the north and middle of the western transect. Here, solar warming was clear resulting in stronger stratification in the northwestern polynya than in the central polynya and close to the Ross Ice Shelf. The warmer water with lower oxygen at >150 m depth at the northern end of the central polynya transect (Fig 1.4) suggest inflow of warm modified CDW onto the continental shelf.

High phytoplankton biomass > 5 µg L^{-1} was observed in surface waters throughout the polynya in both the central and the western transect. In the central polynya and to the south phytoplankton was distributed throughout the upper 50 m of the water column (Fig 1.4 and 1.5). In contrast, in the northwest where thermal stratification was stronger high biomass was distributed throughout the upper 25 m (Fig 1.4). Surprisingly, FlowCAM analysis revealed that the phytoplankton biomass was dominated by diatoms throughout the water column in most of the polynya. The exception was the region around Sta 20 and 33 in the central polynya, that was dominated by *P. antarctica* when sampled on Dec 22 and 23, 2013, and *P. antarctica* was still dominant when Sta 33 was reoccupied on Jan 5, 2014. Dissolved iron concentrations were low in surface waters throughout the polynya suggesting iron may be limiting phytoplankton growth (see section 6). Iron limitation was confirmed by all four bioassay experiments in the polynya where iron additions resulted in increased biomass when compared to control conditions without any additions (see section 3).

1.3 Antarctic Circumpolar Current (ACC) bloom

We identified an area of unusually high phytoplankton biomass in the south of the ACC region (Fig 1.6) and sampled the water column to study the factors that contributed to this high biomass. The ACC bloom showed high biomass between 76°30 S and 77° 30 S (Fig 1.6 and 1.7) and spanned an area of at least 10,000

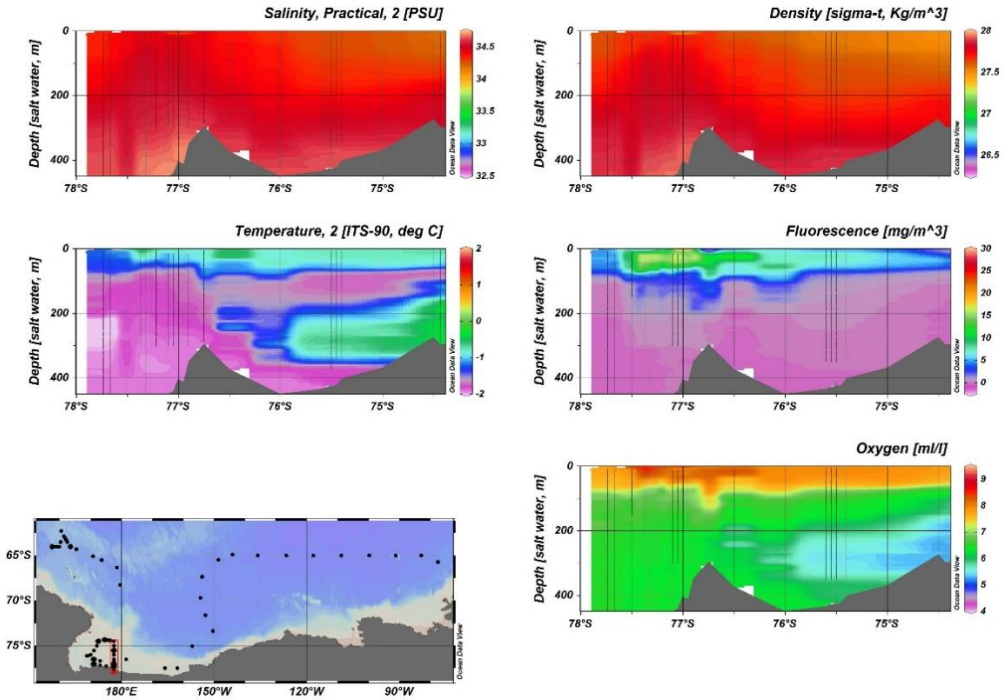

Figure 1.4. Section plots of the south-north transect through the central Ross Sea Polynya. Salinity, Temperature, Density (σ_T), Fluoresence and Oxygen from CTD sensor data plotted versus latitude, note that the scales on the y-axis are the same for all figures. High phytoplankton biomass was observed in the top 40 m of the water column throughout the central transect, with the highest Chl *a* concentrations south of 76°S.

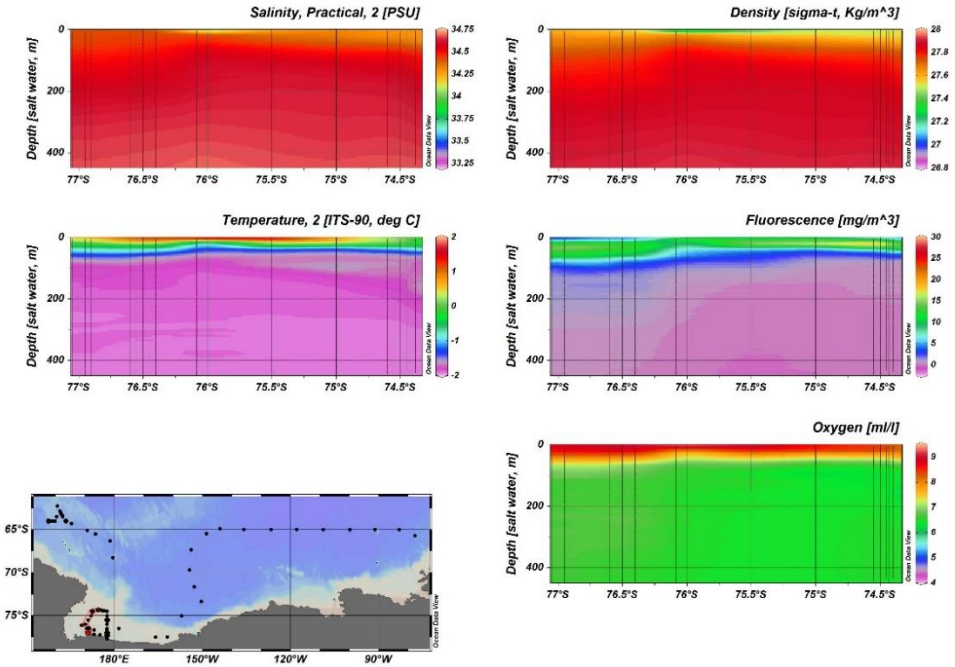

Figure 1.5. Section plots of the north south transect through the western Ross Sea Polynya. Salinity, Temperature, Density (σ_T), Fluorescence and Oxygen from CTD sensor data plotted versus latitude.

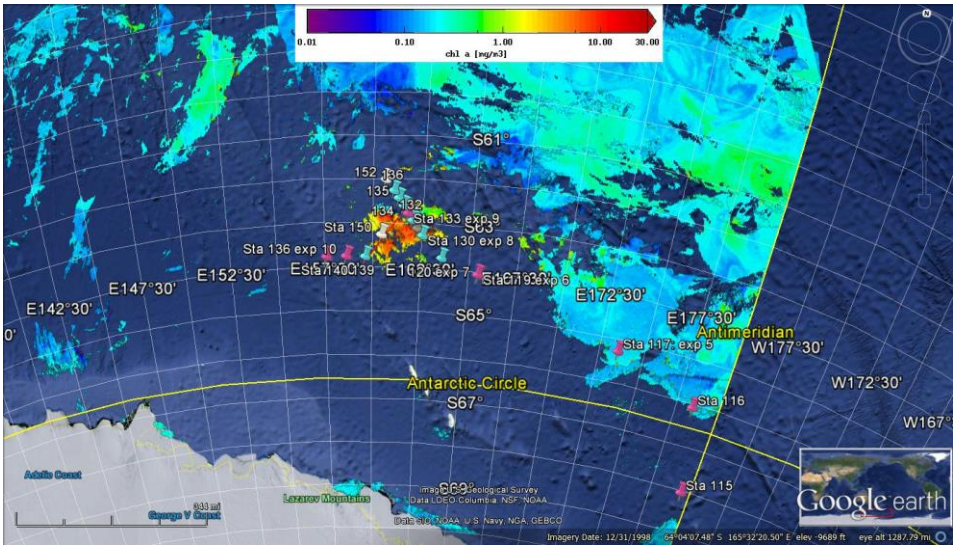

Figure 1.6. Stations sampled in the south of the Antarctic Circumpolar Current (ACC) in a region of high chlorophyll identified from satellite data. Purple stations were dominated by diatoms, white stations by *Phaeocystis antarctica* and blue stations had a mixed phytoplankton population. The high biomass area had a mostly mixed phytoplankton of *P. antarctica* and diatoms, whereas the low biomass stations outside the bloom were dominated by diatoms.

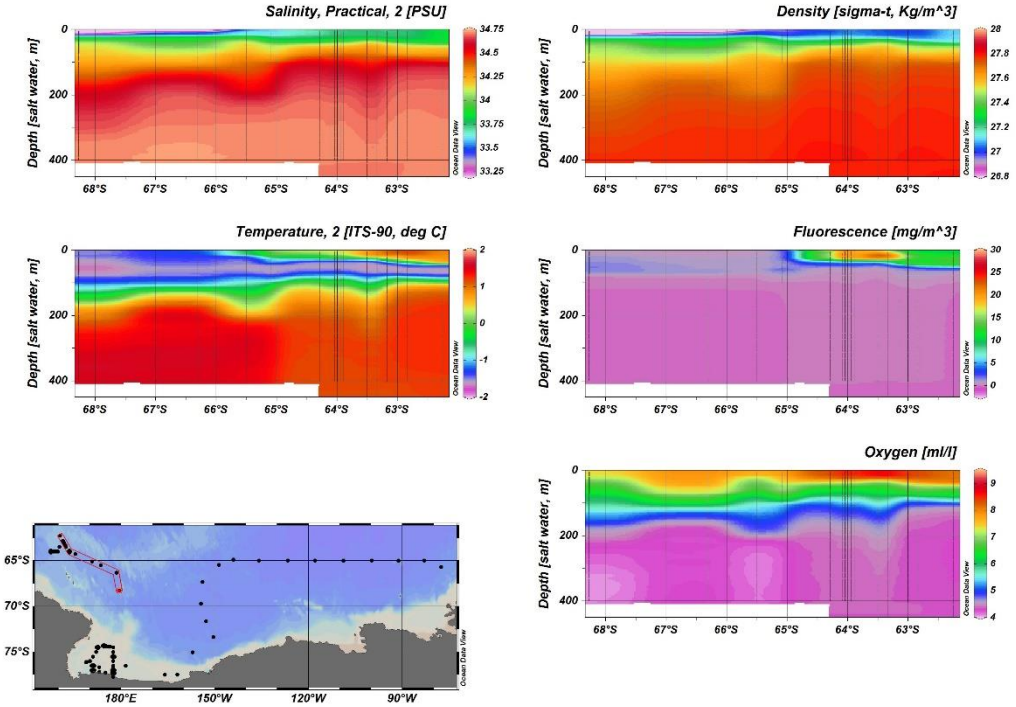

Figure 1.7. Section plots of a south-to-north transect from the sea ice zone (two southern stations) through the ACC bloom. Salinity, Temperature, Density (σ_t), Fluorescence and Oxygen data from the CTD sensors are plotted versus latitude. Sea ice melt waters affect surface waters of the southern stations mostly, resulting in strong stratification. In the northern part solar warming of surface waters were apparent. The highest biomass was found in intermediate surface salinity and intermediate surface solar warming.

square nautical miles (>100 nm cross section). We sampled two diagonal transects to characterize the physical and chemical parameters as well as the phytoplankton community both inside and out of the patch.

The transect from the sea ice zone north of the RSP through the ACC bloom showed sea ice melt influences in surface waters as low salinity (<33.8), especially in the southern most stations (salinity <33.5)(Fig 1.7). This resulted in strong stratification of the upper water column, especially in the southern stations with low phytoplankton biomass where stratification was stronger than in stations in the ACC bloom with high biomass.

The phytoplankton biomass in the ACC bloom was similar to that in the Ross Sea Polynya with similar Chl *a* concentrations (> 6 μg L^{-1}), whereas it was very low in the marginal ice zone (<0.6 μg L^{-1}). This high biomass is very unusual for this region, where phytoplankton growth is generally limited by low iron availability. Also unexpected was that *P. antarctica* comprised a major part of the phytoplankton population in the bloom and dominated several stations (see also section 5). Small diatoms that are generally dominating this area dominated the phytoplankton population outside the bloom. Dissolved iron concentrations were generally low throughout the water column, however, elevated dissolved iron concentrations were measured down to 1800 m depth in the bloom (see section 6). This elevated iron likely fuels the iron requirements of the bloom, however, at present it is unclear what the source of this iron is. Finally, The ACC bloom showed the highest concentrations of the dimethylsulfide (DMS) measured in this region as well as measured on the NBP13-10 cruise (see section 10). This suggests the ACC bloom may be important not only in terms of primary productivity in this region, but also in the sulfur cycle.

1.4 Acknowledgements

We would like to thank the Antarctic Support Contract (ASC) staff on board (see appendix B) and in the office for their excellent technical and logistic support before, throughout, and after the cruise. Their professionalism allowed us to make efficient use of our research time and collect high quality data. Furthermore, Captain John Souza, officers, and crew of Edison Chouest Offshore (ECO) are acknowledged for their excellent support, especially for their efforts during ice breaking and subsequently to maximize fuel efficiency. Thanks to everyone who gave talks during the cruise and shared data and photographs through the local server system. The primary financial support for this work has come from the National Science Foundation to Stanford and MBL. Other institutes and agencies that contributed include the Royal Netherlands Institute of Sea Research (NIOZ), the Netherlands; University of Rhode Island; NASA; Woods Hole Oceanographic Institution; University of British Columbia (UBC), Canada; Moss Landing Marine Laboratory; Swedish University of Agricultural Sciences (SLU), Sweden; Monash University, Australia. Finally, thanks to all friends and family for their support while we enjoyed the Austral summer.

2. CTD operations and sensor calibration

Kate Lowry & Gert van Dijken

Over the course of the cruise we occupied 152 stations: 15 during our transit from Rothera to the Ross Sea, 99 in the Ross Sea, and 38 in the ACC following the Ross Sea. There were a total of 202 CTD/rosette casts performed using both the Trace Metal Clean (TMC) CTD package (72 casts) and the conventional CTD package (130 casts). The total number of Niskin bottles closed was 1744, which corresponds to approximately 20,000 liters of seawater collected. Of the total number of stations, 50 were full 'daily' stations and approximately 80 were sensor-only casts where water samples were not taken. There were 14 TMC casts that were used only for iron (Fe) measurements, comprising a total of four transects to map iron distributions. A total of eight TMC casts were used exclusively for collecting water for the bioassay experiments.

At each of the 50 'daily' stations, water was collected from 5 to 6 depths in the upper 100 meters of the water column for biological sampling and at an additional 6 to 7 depths below 100 meters using the Niskin bottles on the CTD rosette. The standard desired depths in meters for biological sampling were 2 (i.e. surface), 10, 25, 50, 75, and 100 meters; however, the actual depth varied based on sea surface conditions and/or the presence of strong gradients or a fluorescence maximum that resulted in an occasional shift of one of the standard sampling depths. The surface bottle was especially prone to omission or shifting due to heavy seas that prevented sampling in the upper 5-10 meters. Below 100 meters, the standard depths were 200, 300, and 400 meters in deep waters and additional bottles within 10-15 meters from the bottom and 20-25 meters from the bottom in the Ross Sea. When additional Niskin bottles were available, higher resolution sampling was performed (i.e. 250 m, 350 m, etc.) through the water column. Generally, the first cast at each daily station was a TMC cast for core sampling, followed by a conventional CTD cast to collect additional water at two depths. The naming convention for stations is the station number followed by an underscore and the cast number.

During TMC casts, the CTD/rosette was prepared by the science team and the MTs and deployed from the deck outside of the Trace Metal Clean van. During conventional casts, the MTs prepared the CTD and it was deployed from the Baltic Room. The ship's crew handled the winch operations for all CTD deployments. After the CTD entered the water it was lowered to 10 meters (or 15 in heavy seas) and allowed to soak for 5 minutes or longer in order for the sensors to stabilize. Usually the cast was began only after the primary and secondary salinity, temperature, and oxygen sensors reached close agreement; however, there were some instances where the sensors only stabilized upon being lowered deeper into the water column. After the 5+ minute soak, the CTD was brought up to the minimum depth allowed (up to 2 meters) and after 10 seconds of waiting, data recording commenced and the cast was lowered to the bottom depth of the cast. Niskin bottles were fired on the up cast only after waiting 20 – 25 seconds for the water column to stabilize before firing a bottle at the desired depth. When multiple bottles were fired at one depth, the bottles were fired a few seconds apart.

Data recorded from the CTD profiles include temperature, salinity, oxygen, fluorescence, beam transmission, PAR/irradiance, surface PAR, and sound velocity. The fluorescence and beam transmission data are not directly comparable between the TMC and conventional CTD sensors and thus these data should be treated separately.

Salinity and oxygen samples were taken from the TMC and the conventional CTD as well as the underway system for sensor calibration. In total, there were 80 oxygen samples taken, with 52 from the TMC CTD, 23 from the conventional CTD, and 5 from the underway system. There were 98 salinity samples taken, with 53 from the TMC CTD, 28 from the conventional CTD, and 17 from the underway system. The oxygen samples were analyzed on the Langdon Oxygen Amperometric Titrator and the salinity samples were analyzed on the Guideline Autosal. Both instruments were functioning well on the cruise after some initial startup difficulties. Oxygen samples were stored at room temperature with water in the flask well until analysis and salinity samples were stored at 21˚C until analysis. Salinity standards were run at the beginning, in the middle, and at the end of each salinity run to ensure the accuracy of the salinity readings.

Figures 2.1 and 2.2 show how the primary and secondary sensors compared with each other (left panels) and with the measured values (center and right panels) over the course of the cruise for both the conventional (top) and the TMC (bottom) CTDs. The primary sensors are labeled as CTDSAL_UP and CTDOXY_UP in the figures below and are plotted against measured values in the center, while the secondary sensors are labeled as CTDSAL2_UP and CTDOXY2_UP and plotted against measured values on the right.

As shown in figure 2.1 and 2.2, the salinity sensors for both the TMC and the conventional CTD compared well with each other and with the measured values. There are occasional values off of the 1:1

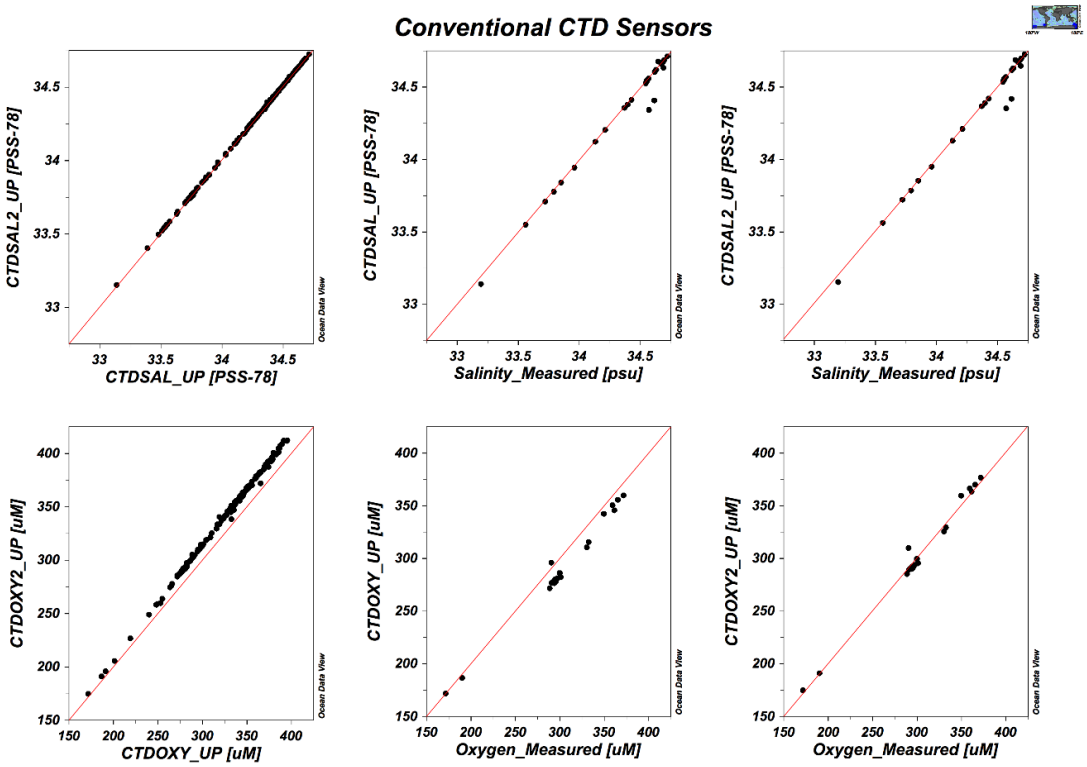

Figure 2.1. Sensor data of primary and secondary sensors of the conventional CTD plotted against each other (left two panels) and against measured data (right four panles).

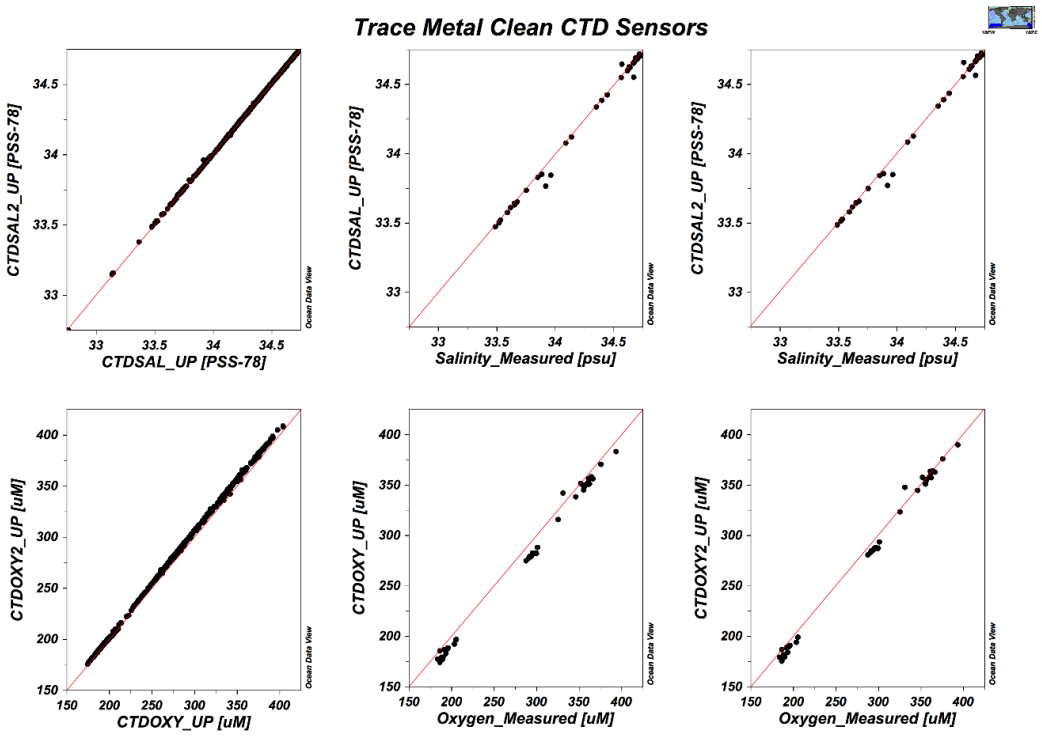

Figure 2.2. Sensor data of primary and secondary sensors of the trace metal clean CTD plotted against each other (left two panels) and against measured data (right four panles).

line (depicted in red) that are likely due to measurement error, but the majority of samples match the both the primary and secondary sensors very well. Conversely, the primary and secondary oxygen sensors do not follow each other exactly, with increased drift at high values especially in the case of the conventional CTD. In both cases, the measured oxygen values match the secondary sensors better than the primary sensors. This noticeable difference is likely due to the fact that the primary sensors were used on a previous cruise and have thus had more exposure to oxygen that results in a decreased sensitivity. Although there are some values that deviated more substantially from the 1:1 line, most measured values were within a few µM of the sensor values indicating reasonable accuracy. In the case of the TMC CTD, the secondary oxygen sensor was about 5 µM lower than the measured values. Drift over time will be assessed more fully after the cruise, but based on the data shown below, there does not seem to be much drift in the sensors over the course of the cruise.

Results from the underway data show that the oxygen sensor underestimates by 50 – 60 µM relative to measured values (comparable to the 35-40 µM underestimation found in March 2013 on a different cruise). The sea surface salinity sensor was found to underestimate sea surface salinity by approximately 0.05 psu, with TSG 2 performing slightly better than TSG 1. Drift was observed in both TSG sensors over the cruise.

Table 2.1. Trace metal clean CTD sensors and equipment

Sensor	Serial Number	Last Calibrated	Comments
CTD Fish	09P55620-0987	12/13/2012	
CTD Fish Pressure	116284	12/13/2012	
CTD Deck Unit	11P19858-0490	N/A	
Slip-Ring Assembly	213773	N/A	Installed 20-Nov-13
Carousel Water Sampler	3255620-0731	N/A	
Pump (primary)	055644 3.0K	11/28/2010	Installed 20-Nov-13
Pump (secondary)	051646 3.0K	4/6/2011	Installed 20-Nov-13
Temperature (primary)	03P5097	6/12/2013	Installed 20-Nov-13
Temperature (secondary)	03P5090	6/12/2013	Installed 20-Nov-13
Conductivity (primary)	042067	6/12/2013	Installed 20-Nov-13
Conductivity (secondary)	040926	6/12/2013	Installed 20-Nov-13
Dissolved Oxygen (primary)	2512	12/14/2012	Installed 20-Nov-13
Dissolved Oxygen (secondary)	2267	6/12/2013	Installed 20-Nov-13
Altimeter	60145	N/A	Installed 20-Nov-13
Transmissometer	CST-1581DR	12/4/2012	Installed 20-Nov-13
Fluorometer	FLRTD-1482	7/17/2013	Installed 20-Nov-13
PAR	4721	10/26/2012	Installed 6-Dec-13 (failed 10-Jan on cast 118)
PAR	4361	07/03/13	Installed 11-Jan-13

Table 2.2. Conventional CTD sensors and equipment

Sensor	Serial Number	Last Calibrated	Comments
CTD Fish	09P70675-1130	12/11/2012	
CTD Fish Pressure	120089	12/11/2012	
CTD Deck Unit	11P19858-0490	N/A	
Slip-Ring Assembly	1406	N/A	
Carousel Water Sampler	3214153-0140	N/A	
Pump (primary)	051627 3.0K	12/23/2012	Installed 20-Nov-13
Pump (secondary)	051626 3.0K	12/23/2012	Installed 20-Nov-13
Temperature (primary)	03P2308	6/28/2013	Installed 20-Nov-13
Temperature (secondary)	03P2299	6/12/2013	Installed 20-Nov-13
Conductivity (primary)	042069	6/18/2013	Installed 20-Nov-13
Conductivity (secondary)	042067	6/12/2013	Installed 20-Nov-13
Dissolved Oxygen (primary)	0161	6/12/2013	Installed 20-Nov-13
Dissolved Oxygen (secondary)	0080	2/13/2013	Installed 20-Nov-13
Altimeter	42434	N/A	Installed 20-Nov-13
Transmissometer	CST-889DR	9/5/2013	Installed 20-Nov-13
Fluorometer	AFLD 011	7/17/2013	Installed 20-Nov-13
PAR	4721	10/26/2012	Installed 20-Nov-13
PAR	4361	07/03/13	Installed 8-Dec-13

3. Bioassay experiments- Iron and light availability to phytoplankton

Anne-Carlijn Alderkamp and all cruise participants

The interactive effects of the availability of iron (Fe) and light on phytoplankton photosynthesis rates and characteristics, biochemical composition, and gene expression were investigated 10 bioassay experiments in the Ross Sea Polynya (RSP) and in or near the Antarctic Circumpolar Current (ACC, Figure 3.1). The four experiments in the RSP consisted of both Fe and light manipulations, whereas only Fe additions were tested in the six ACC experiments.

3.1 Methods

Using the trace metal clean rosette and CTD system, surface water (10 m) was obtained at ten stations (four in the Ross Sea and six in the ACC, Fig 3.1) and phytoplankton was incubated in deck incubators with and without the addition of Fe. Trace metal clean techniques were used throughout the experiments and sampling. Iron was added to the +Fe treatments and 2 L polycarbonate experiment bottles were incubated at in situ surface water temperature. In the Ross Sea, the experiments were carried out at two different light levels and deck incubators were screened to achieve 5% (LL, low light) and 30% (HL, high light) of the incident irradiance. At day 4 and 6, bottles were taken out and the entire volume was subsampled for a suite

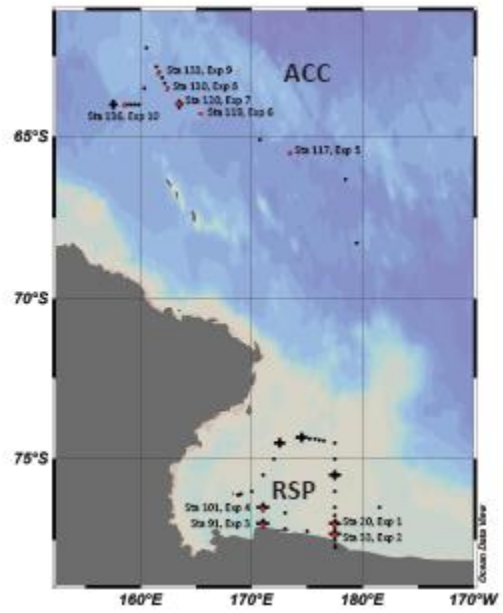

Figure 3.1 Location of the 10 bioassay experiments. Experiments 1-4 in the Ross Sea Polynya consisted of an iron addition (+Fe) and control treatment C, (no additions) and were incubated at two different light levels (5% and 30% of incident irradiance. Experiments 5-10 in or near the ACC consisted of just +Fe and C treatments.

of parameters (see table 3.1). In the ACC, the experiments were carried out at HL only, and sampled at day 4.

3.2 Preliminary results

Phytoplankton growth was observed as an increase in Chl *a* in almost all experiments (Fig 3.2 top panels). Moreover, Fe-additions enhanced phytoplankton growth in all four experiments in the Ross Sea at both high and low light incubations. In the Ross Sea, Fe effects on Chl *a* were most pronounced in the low light incubations, where Chl *a* concentrations reached > 25 µg L^{-1} in the experiments on Sta 20 and 33. The Fv/Fm was higher in all +Fe treatments when compared to the controls in the Ross Sea experiments (results not shown).

Fe-effects on Chl *a* concentrations were less clear in the ACC stations (Fig 3.2 bottom panels). Fe-additions resulted in higher Chl *a* when compared to the control treatments in Sta 130 and 133 in the bloom, but there were no significant effects in other stations within the time frame of our incubations (4 days). Similar to the Ross Sea, Fe-additions resulted

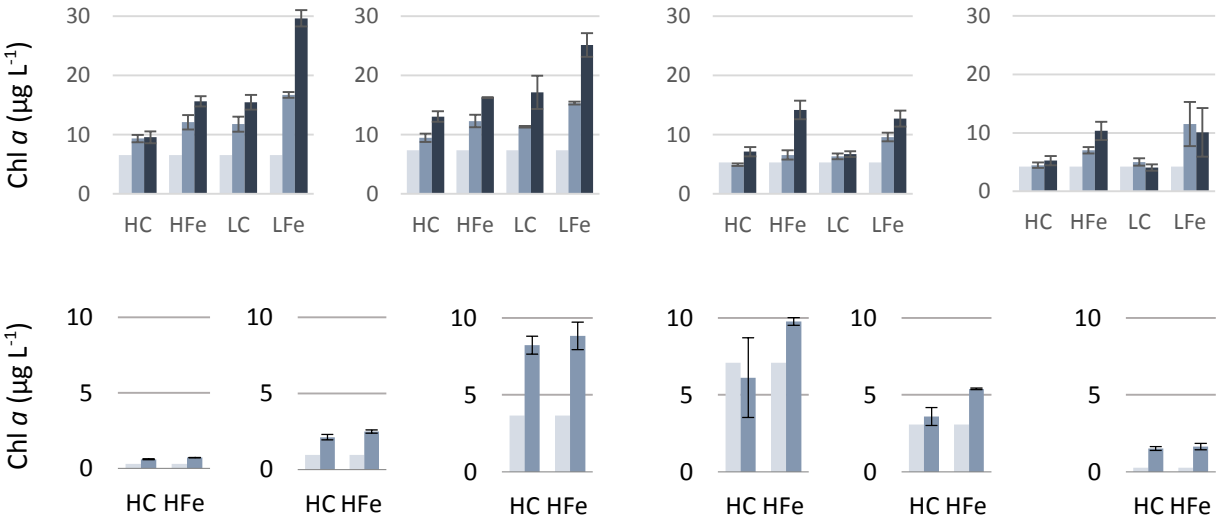

Figure 3.2. Chl *a* concentrations (mean and standard deviation of triplicate experiment bottles) at initial (light grey), day 4 (medium grey), and day 6 (dark grey), of the Fe-addition bioassay experiments for high light (H, 30% of incident irradiance), low light (L, 5% of incident irradiance), control (C, no additions) and Fe addition (Fe, 4 nM dFe additions) conditions.

in a higher Fv/Fm in almost all experiments when compared to the controls, suggesting physiological acclimation of the phytoplankton to increased Fe concentrations in these experiments.

The measurement of both physiological and transcriptomic parameters at day 4 and 6 (Ross Sea experiments) and day 4 (ACC experiments) allows us to study phytoplankton responses to changes in their Fe and light availability on both the genetic and phenotypic level and link genetic responses to physiological parameters. These data will also be helpful in interpreting physiological and transcriptomic signals from phytoplankton sampled at the stations.

Table 3.1. Physiological, chemical, and genetic parameters measured in the bioassay experiments.

Measurement	**Institute**	**Measurement description (section)**
Chl *a* concentration	Stanford	4
Variable Fluorescence (Fv/Fm, σPSII, and *p*)	Stanford	4
Phytoplankton pigment composition (HPLC)	Stanford, University of Groningen	4
Particulate carbon, nitrogen	Stanford	4
Sulfur cycle components (DMS, DMSP, DMSO)	Stanford, UBC, WHOI	10
Phytoplankton community composition (Flowcam)	Stanford	5
Photosynthesis vs irradiance characteristics	Stanford	4
Particle absorption	Stanford	4
Phytoplankton gene expression (transcriptomic analysis)	MBL	7
Nutrients (nitrate, nitrite, phosphate, silicate,)	Royal NIOZ	4
Dissolved Fe	Royal NIOZ	6
Proteome analysis	SLU	15
Hydrogen peroxide concentrations	MBL	13

4. Core phytoplankton data

Kate Lowry, Kate Lewis, Gert van Dijken and Anne-Carlijn Alderkamp

A series of core phytoplankton data were collected to provide physiological background data for all measurements in the Phantastic program. At each core depth in the upper 100 meters, samples were collected for phytoplankton pigment analysis via high performance liquid chromatography (HPLC), and Chlorophyll *a* (Chl a) concentrations via fluorometry, particulate organic carbon and nitrogen (POC/N) elemental composition, and variable Chl fluorescence via fluorescence induction and relaxation (FIRe) and Pulse Amplitude Modulation (PAM) fluorometry. Additionally, at two depths from each station (typically 10 and 50 meters or the deep chlorophyll maximum, if present), samples were also collected for phytoplankton absorption spectral analysis (Ap/Ad) and fixed in gluteraldehyde for cell counts. The sampling depths for this analysis were chosen to match those of the photosynthesis versus irradiance (PvE) curves. Core biological sampling was also performed at each time point for the bioassay experiments. In total, there were ~500 samples collected for HPLC analysis, ~600 samples for POC/PON analysis and

variable fluorescence, ~1800 samples for Chl *a* concentration, and ~165 samples for carbon uptake and phytoplankton absorption spectra.

4.1 Filtrations for pigments and elemental composition (Kate Lowry and Kate Lewis)

Phytoplankton particles for each sample type were collected by filtering seawater through Whatman glass-fiber filters (GF/F) with a diameter of 24 mm and a nominal pore size of 0.7 µm over low vacuum pressure (<150 mm Hg). The filters used for POC/N analysis were combusted prior to use in an oven at 450˚C for 4 hours. Following filtration, the POC/N samples were dried in an oven at 60˚C for 24 hours and stored at room temperature. After the cruise, the POC/N samples will be packed and prepared for elemental analysis, along with several seawater blanks that were also collected during the cruise. Phytoplankton pigment samples were immediately frozen after filtration in liquid nitrogen and stored at -80˚C and will remain at that temperature until HPLC analysis. Preserved seawater samples were collected at two depths per station by fixing 50 ml of seawater with 1 ml of 50% gluteraldehyde and stored at +4˚C. These samples will be analyzed for counts of phytoplankton abundance at Stanford University.

Chl *a* concentration and Ap/Ad samples were analyzed onboard the ship. Chl *a* samples were collected in triplicate and extracted in 5 mL of 90% acetone at +4˚C in the dark for 24 hours prior to reading before and after acidification on a Turner Designs fluorometer. Chl *a* was also analyzed at two corresponding depths from the conventional CTD to assess agreement between the duplicate casts. Depth-integrated Chl *a* was calculated and vertical profiles were plotted at each station. Typical profiles from the Ross Sea, ACC, and ACC bloom are presented in Fig. 4.1.

Samples collected for particle absorption (Ap) were run immediately on the spectrometer and then extracted twice in 80% methanol for at least 5 minutes per extraction followed by two seawater rinses and run again on the spectrometer to provide the absorption by detritus (Ad). Phytoplankton absorption spectra were calculated by subtracting detrital absorption from the particulate absorption from 300 to 800 nm.

Filtrate for each sample was collected for nutrient analysis after the cruise by the Royal NIOZ. Samples for analysis of nitrate, nitrite and phosphate was stored at -20°C, samples for silicate analysis was stored in the dark at +4°C to prevent precipitation.

4.2. Photosynthesis versus Irradiance Curves (Gert van Dijken)

We studied the characteristics of photosynthesis by natural phytoplankton assemblages at different light levels by performing so-called PvsE curves (photosynthesis vs. irradiance). These were used to determine maximum photosynthetic rates, the light intensity to which phytoplankton is adapted, light limited rates of photosynthesis and photoinhibition parameters. During this cruise a total of 163 PvsE curves were done from two depths at each 'daily' station. These depths were normally 10 m (the same depth at which the bio-assay experiments were started) and the depth of the chlorophyll maximum.

In short, 13-14 20 mL PET scintillation vials were filled with 2 mL of seawater. Radiolabelled bicarbonate ($H^{14}CO_3$) was added before the vials were transferred into a photosynthetron where they were incubated for 2 hours at 0°C under different light conditions, ranging from 2 to >600 µEin m^2 s^{-1}. After incubation, 100 µL of 6 N hydrochloric acid was added and the vials were gently shaken for around 24 hours to drive off inorganic carbon. After neutralization with 100 µL 6N sodium hydroxide, 10 mL of scintiallation cocktail (Ecolume) was added. The samples were then counted for 5 minutes on a liquid scintillation counter.

For each PvsE curve phytoplankton was filtered onto a GF/F filter to generate an absorption spectrum (Ap) of phytoplankton pigments on a Perkin Elmer UV/VIS Lambda 18 spectrophotometer with an integrating sphere from 300-800 nm. This spectrum will be used to quantify the amount of light absorbed during the PvsE incubation and subsequently to calculate the quantum yield of photosynthesis. Detrital absorption (Ad) was also measured after extraction of the sample in 80% methanol.

4.3. Simulated in situ production (Gert van Dijken)

In addition to the 'standardized' PvsE experiments simulated in situ production was estimated. During these experiments carbon fixation by natural phytoplankton is measured by incubating samples in an outside

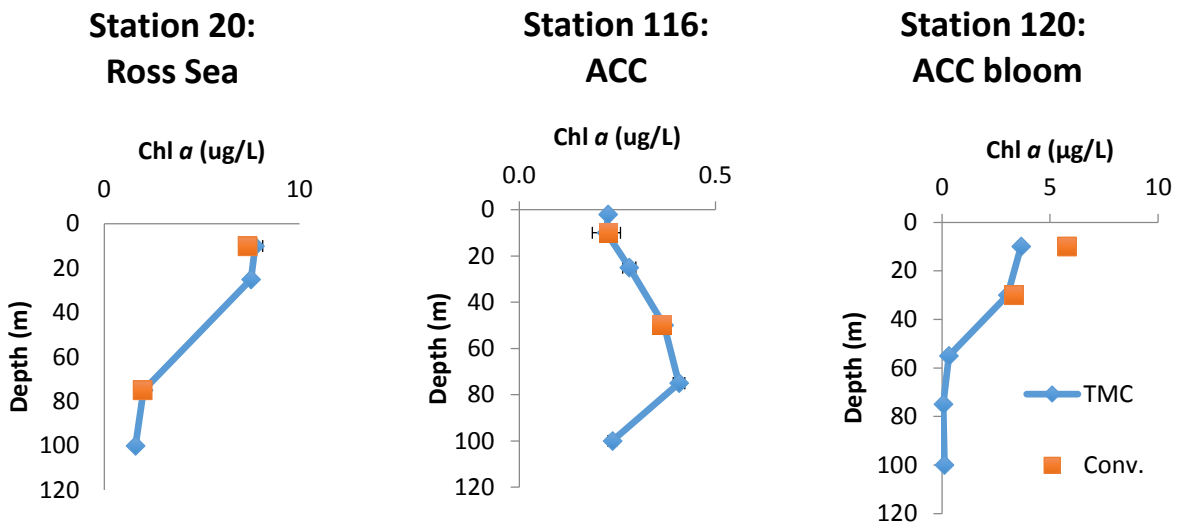

Figure 4.1. Typical Chl *a* (ug/L) vertical profiles for the Ross Sea Polyna, Antarctic Circumpolar Current (ACC), and the *P. antarctica* bloom in the ACC. Note the different scales for Chl *a* concentrations on the y-axis.

incubator for 24 hours under different light levels. With these experiments photosynthesis at different depths in the water column can be estimated and a daily column integrated primary production rate can be calculated. A total of 38 simulated in situ experiments were performed.

In short, Falcon flasks (250 mL) were filled with 150 mL of seawater sample. After this radiolabelled bicarbonate ($H^{14}CO_3$) was added. In order to simulate light attenuation in the water column the samples were covered with different layers of neutral density screening. The following optical light levels were used: 85% (no screening), 65%, 25%, 10%, 5% and 1%. Care was taken to select the sample from the appropriate Niskin bottle collected closest to the optical depth at which it was incubated. After 24 h incubation time 30 mL of sample was filtered in triplicate over GF/F filters. The filters were acidified with 100 µL of 6N hydrochloric acid to drive off inorganic carbon. After addition of 5 mL of scintillation cocktail (Ecolume) the samples were counted on a liquid scintillation counter.

4.3 Variable Chlorophyll Fluorescence (Anne-Carlijn Alderkamp)

Variable Chl fluorescence was determined on a PAM fluorometer (Water-PAM, Heinz Walz, GmBH, Germany) to determine the maximum efficiency of photosystem II (Fv/Fm) according to Krause and Weis (1991) and a FIRe fluorometer (Satlantic LP, Canada) to determine Fv/Fm, functional absorption cross section (σPSII), and energy transfer between PSII units (*p*) according to Gorbunov et al. (1999). Samples were dark-acclimated for at least 30 min on ice prior to analysis and both the PAM and FIRe fluorometer were blanked with filtered seawater prior to measurements.

5. Phytoplankton species characterization by Flowcam

Hannah Joy-Warren

The FlowCAM was used to estimate community composition at daily stations and to scope out locations for beginning experiments. Samples were imaged on the FlowCAM at two magnifications (40x and 100x). Samples imaged with the 4x objective lens were run using a 300 µm flow cell and pre-filtered at 300 µm, and samples imaged with the 10x objective were run on a 200 µm flow cell and pre-filtered at 200 µm. The

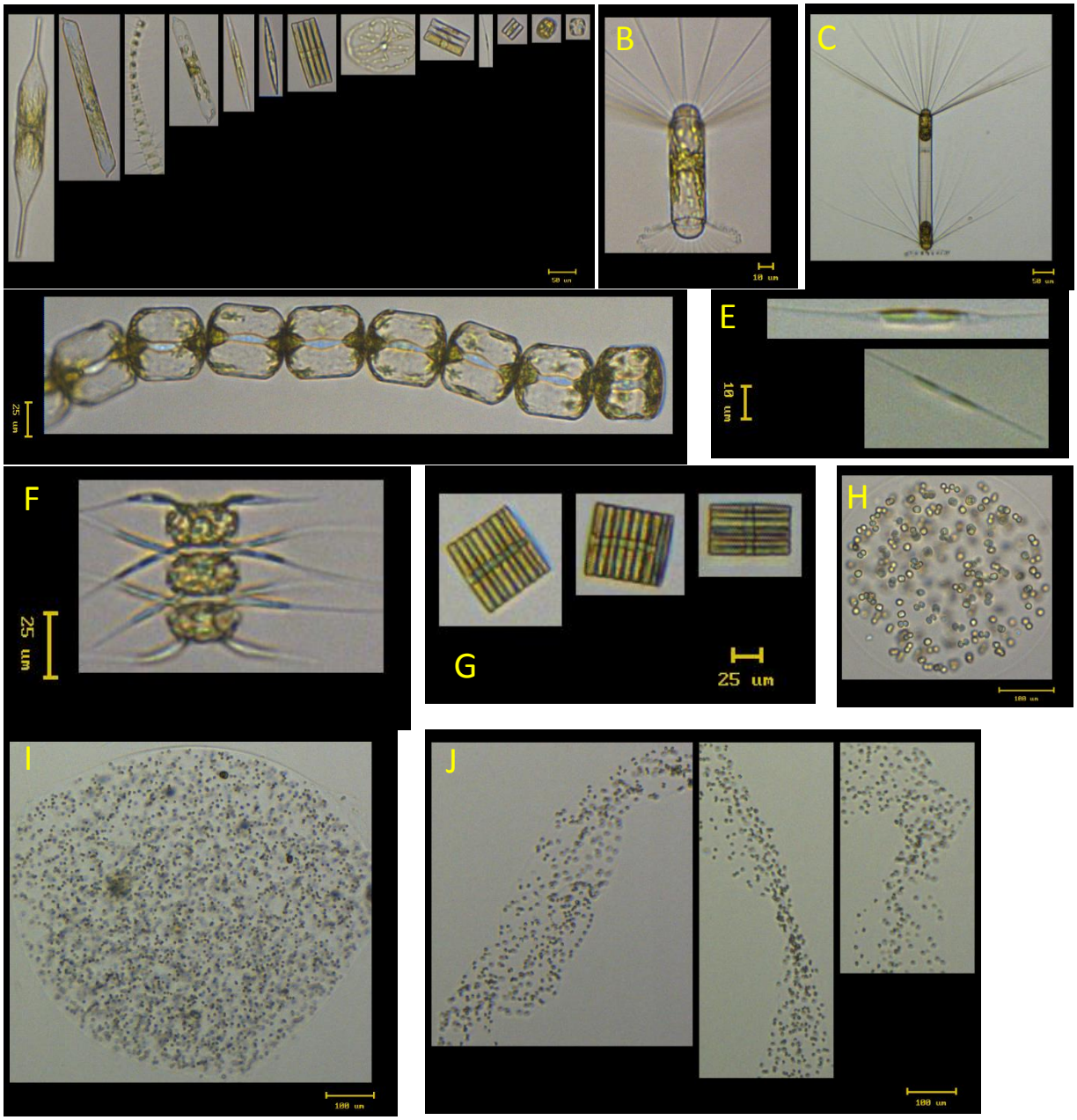

Figure 5.1 Various phytoplankton cells imaged by the FlowCAM at different magnification. A) Diatom diversity; B & C) *Corethron* sp.;, D) centric diatom chain; E) Pennate diatoms, F) *Chaetoceros* sp. G) *Fragilariopsis* sp. ; H, I, & J) Various shapes and sizes of *Phaeocystis antartcica* colonies.

FlowCAM was focused manually using COUNT-CAL™ Particle Size Standard 50 µm beads (Thermo Scientific). Samples were run until a minimum of 1000 images were collected. The flow cell was flushed with Milli-Q water between samples. When flow cells accumulated stuck particles, the flow cell was filled with a 10% Liquinox solution and sonicated for 15 minutes. Flow cells were flushed with Milli-Q before using.

At daily stations, water was analyzed from three depths (10 m., deep chlorophyll maximum or 50 m., and 100 m.) to observe the shifting community composition through the water column as well as along our cruise transect. We were also able to compare the phytoplankton community composition between the Antarctic Circumpolar Current and the Ross Sea Polynya. An example of the diatom diversity observed is

shown in Fig 5.1A. Common diatoms observed include *Corethron sp.* (Fig 5.1 B & C), *Fragilariopsis sp.* (Fig 5.1 G), centric diatoms (Fig 5D), *Chaetoceros sp.* (Fig 5G), and pennate diatoms (Fig 5E). Diversity in *Phaeocystis* colony morphology was also observed (Fig 5 H, I, & J).

To estimate the community composition at a station prior to beginning a bioassay experiment, we ran a FlowCAM sample from the deep chlorophyll maximum. We were immediately able to determine whether the phytoplankton community at the station was *Phaeocystis*-dominated, diatom-dominated, or mixed. The community composition informed decisions about where to begin experiments such that we had a series of experiments beginning with *Phaeocystis* -dominated, diatom-dominated, and mixed communities. Samples from each experiment were run on the FlowCAM on sampling days. Based on preliminary observations, the particle density increased over time during experiments. Particle density was higher in high light treatments than in low light or dark treatments. Particle density was also generally higher in +Fe treatments.

6. Trace metal measurements

Loes J. A. Gerringa, Patrick Laan and Hein J.W. De Baar (not on board)

Iron (Fe) has been shown to be a limiting nutrient for phytoplankton growth in Antarctic waters (de Baar et al. 1990; Martin,1994; Coale et al., 1996), even in the productive continental shelves surrounding the Antarctic continent (Arrigo et al., 2003). The abundance of Fe in seawater is controlled by a balance between Fe input (via sediment resuspension, sea-ice and glacial melt, upwelling, atmospheric deposition, hydrothermal inputs and lateral and vertical diffusion from sources), stabilization processes via organic complexation that keep Fe in the dissolved phase, and by removal processes like (oxidative) precipitation, adsorptive scavenging, and phytoplankton uptake (Gledhill and Van den Berg, 1994; Thuróczy *et al.*, 2011, 2012; Klunder *et al.*, 2011; Alderkamp et al., 2012; Gerringa et al., 2012).

Dissolved organic molecules, called ligands, bind Fe. In this way the ligands increase the solubility of Fe, retard the precipitation of Fe (hydr-) oxides and hence increase Fe availability for biological uptake in the upper parts of the Ocean. As such, the binding by dissolved organic ligands may play an important role in the dissolution of Fe and keeping Fe in the dissolved phase. To allow biological utilization of Fe, part of the organically complexed Fe pool must be available for phytoplankton uptake. It is still not clear which part of the organically complexed Fe pool can be directly utilized by phytoplankton and how it is taken up.

Recent work from Sedwick et al. (2011) showed that even in early spring dissolved Fe (DFe) concentrations are extremely low in the surface waters of the Ross polynya. It is unknown which sources of Fe supply the extensive phytoplankton blooms that continue to exist during spring and summer. Former research of this group in the Amundsen polynya proved the Pine Island Glacier to be the main source of Fe (Alderkamp et al. 2012, Gerringa et al. 2012, Thuroczy et al, 2012). Since such a distinct glacier source appears not to be present to supply the large Ross polynya, other sources need to be investigated such as vertical fluxes from the sediment as was found to be an important second source in the Amundsen polynya (Gerringa et al, 2012). Sedwick et al. (2011) suggested aerosol input and ice melt as sources at the surface of the Ross Sea polynya and vertical exchange and reductive dissolution of sediment as sources from below.

Finally, the Phantastic cruise is listed as a GEOTRACES process study. GEOTRACES aims to improve our understanding of biogeochemical cycles and large-scale distribution of trace elements and isotopes in the marine environment and establish the sensitivity of these distributions to changing environmental conditions. The six GEOTRACES key trace elements are Fe, aluminium, (Al), zinc (Zn), manganese (Mn), cadmium (Cd) and copper (Cu). These were selected since they can help to explain and distinguish the possible sources of Fe (Mn, Al) and are of importance for phytoplankton growth (Zn, Cu, Cd).

6.1 Objectives

For the Phantastic project our objectives are four-fold.

1. Identifying the sources of Fe that supply enough DFe to sustain the phytoplankton blooms in the Ross polynya.

2. Qualifying and quantifying the organic speciation of Fe (Fe-binding ligands) to know the capacity of the water to keep Fe in solution and thus more available for phytoplankton. DFe can easily be transported away from a source, e.g. vertically from depth to the photic zone and horizontally to the polynya.
3. Quantifying DFe in bioassay experiments at the same sampling times as the other parameters, in order to link responses of phytoplankton to Fe to actual DFe concentrations.
4. Quantifying the key Geotraces trace elements that can be measured on stored samples: Fe, Zn, Mn, Cd in order to explain and distinguish the possible sources of Fe (compare to Mn concentrations) and their importance for phytoplankton growth (Zn, Cd).

6.2 Methods and equipment

6.2.1 Sampling

All TMC-CTD casts (Table XX) were sampled for DFe and major nutrients NO_3/NO_2, PO_4 and SO_4 at all trace metal depths. All filtering (Sartorius®, 0.2µm; Satrobran 300) was done inside the trace metal van under clean conditions. In addition, filtered and unfiltered samples from selected stations were acidified and stored to determine both dissolved and total dissolvable metal concentrations of the six GEOTRACES key trace metals (Fe, Al, Zn, Mn, Cd, Cu, possibly together with additional metals Co, Ni, Ag) in the NIOZ laboratory by inductively coupled plasma mass spectrometry (ICP-MS). Moreover, experiment bottles from the initial waters and sampling points of control and +Fe treatments of the ten bioassay experiments were sampled for DFe.

6.2.2 Methods for dissolved Fe measurements

Dissolved iron concentrations were measured directly on board by an automated Flow Injection Analysis method (Klunder et al., 2011). Filtered and acidified (Seastar© baseline hydrochloric acid; pH 1.7) seawater was concentrated on a column containing aminodiacetid acid (IDA). This material binds only transition metals and not the interfering salts. After washing the column with ultra-pure water, the column is eluted with diluted acid. After mixing with luminol, peroxide and ammonium, the oxidation of luminol with peroxide is catalyzed by iron and a blue light is produced and detected with a photon counter. The amount of iron is calculated using a standard calibration line, where a known amount of iron is added to low iron containing seawater. Using this calibration line a number of counts per nM Fe is obtained. Samples were analyzed in triplicate and standard deviation are given. Concentrations of DFe measured on the NBP1310 cruise ranged from 12 pM up to 2.767 nM with the median at 0.130 nM for the entire dataset. The standard deviation varied between 0% and 38% (the latter being exceptional), but was generally on average 2.8%. The blank was determined daily by loading a low iron seawater sample for 0 seconds. The blank values ranged from not detectable up to 45 pM. The average limit of detection, 0.007±0.0010 was defined as 3 times

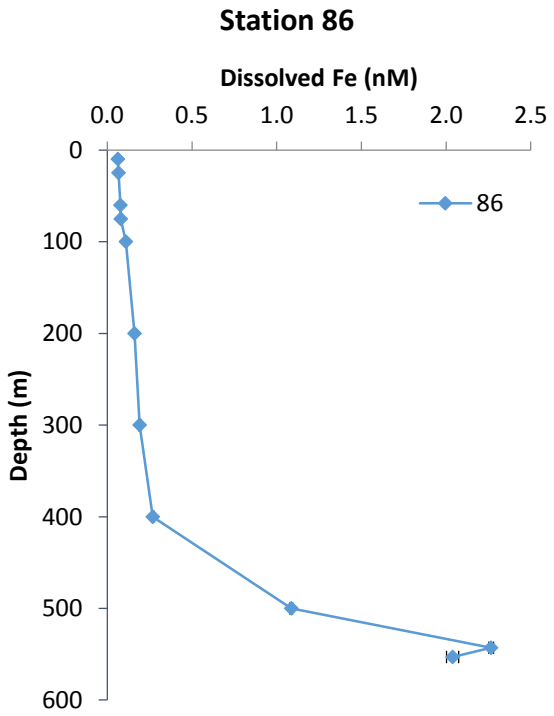

Figure 6.1. Depth profile of DFe (dissolved iron) for station 86 in the Ross Sea polynya. Elevated concentrations near the bottom indicate a source of iron.

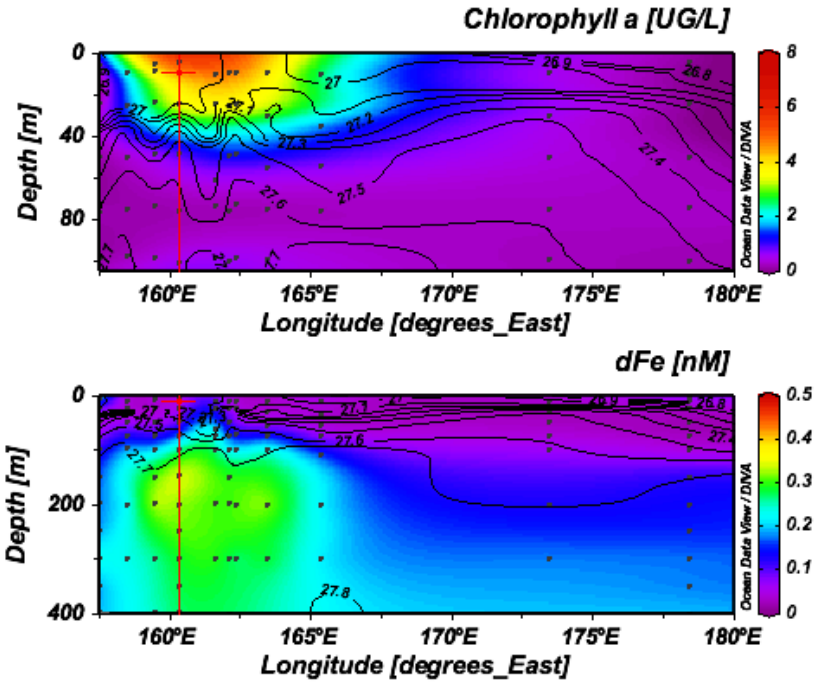

Figure 6.2. Profiles of Chlorophyll a and dissolved iron against depth along a transect in the ACC. Elevated concentrations of dissolved iron were observed under the core of the bloom.

the standard deviation of the mean blank and measured daily.

The consistency of the FIA system over the course of the day was verified using a drift standard. The drift standard was measured several times during the day. The observed drift was less than 5% and no corrections have been made for this drift. A certified SAFe standard (Johnson et al. 2007) for the long term consistency and absolute accuracy was measured at a regular basis.

6.2.3 Organic complexation of Fe

Organic complexation of Fe was determined by Competing Ligand Exchange - Adsorptive Stripping Voltammetry (CLE-AdSV) using 2-(2-Thiazolylazo)-p-cresol (TAC) as a competing ligand (Croot and Johansson, 2000). The binding characteristics of organic Fe binding ligands, the ligand concentration [Lt] (in nanoequivalents of mol Fe, nEq of M Fe) and the conditional binding strength K' (M^{-1}), commonly expressed as log K' are determined The competing ligand TAC with a final concentration of 10 µM was used and the complex (TAC)2-Fe was measured after equilibration (> 6 h) at natural seawater temperatures (2°C) in the dark. The increments of Fe concentrations used in the titration were 0, 0.2, 0.4, 0.6, 0.8, 1.0, 1.2, 1.5, 2, 2.5, 3, 4, 6, and 8 nM. The electrical signal recorded with this method (nA) will be converted into a concentration (nM), then the ligand concentration and the binding strength will be estimated using the non-linear regression of the Langmuir isotherm (Gerringa et al. 1995; 2014 in press).

CLE-AdSV was performed using two setups consisting of a µAutolab potentionstat (Metrohm Autolab B.V., formerly Ecochemie, The Netherlands), a 663 VA stand with a Hg drop electrode (Metrohm) and a 778 sample processor with ancillary pumps and dosimats (Metrohm), all controlled using a consumer laptop running Nova 1.9 (Metrohm Autolab B.V.). The VA stands were mounted on elastic-suspended wooden platforms in aluminium frames developed at the NIOZ to minimize motion-induced noise while electrical noise and backup power was provided by Fortress 750 UPS systems for spike suppression and line noise filtering (Best Power). Sample manipulations were performed in laminar flow cabinets. The DFe concentrations that are necessary for the data interpretation were measured with Flow Injection Analysis (FIA) on board (see section above) in separate samples taken from the bottles sampled for Fe complexation.

6.3 Preliminary results

6.3.1 Objective 1: Fe Sources

DFe was sampled in all TMC-CTD casts, in order to know the DFe distribution in the research area. Although results are still preliminary, it is clear that in the surface concentrations of DFe in the polynya as

well as in the rest of the Ross Sea and the ACC were extremely low (<0.1 nM at 10 meter up to around 0.15 nM at 200 meter), confirming the results of Sedwick et al., (2011). Concentrations increased with depth and were relatively high near the sediment (up to 2nM at station 86, Figure 6.1).

Three special transects were sampled to identify possible Fe sources. Here, specifically total dissolvable Fe (the fraction of Fe in unfiltered samples that becomes dissolved during 6 month at pH=1.7) was sampled as well. The transects were located as follows:

- Transect 1 to study the influence of the Ross Ice Shelf and the banks: south to north at 177° 30 E, from the Ross Ice shelf via a trough up to the Ross Bank
- Transect 2 to study the influence of the banks: east to west from the Pennell bank into the Joides Trough
- Transect 3 to study the influence of land: from west to east from Franklin Island to Joides Trough.

Furthermore the non-treated CTD data (not binned) will be used to calculate the vertical turbulence in order to estimate vertical diffusive fluxes from the sediments to the photic layer.

Sampling continued after the ship left the main research area of the Ross Sea polynya. In this part of the ACC a Phaeocystis bloom was located and sampled extensively. The daily biological sampling of the first 200 meters suggested elevated dissolved iron numbers at subsurface below the Chlorophyll maximum as shown in figure 6.2 (figure made by Kate Lowry). Therefore we conducted 2 deep stations to 2000 meters depth, one inside the core of the Chl *a* region (station 150) and one outside the maximum (station 140, Fig 6.3).

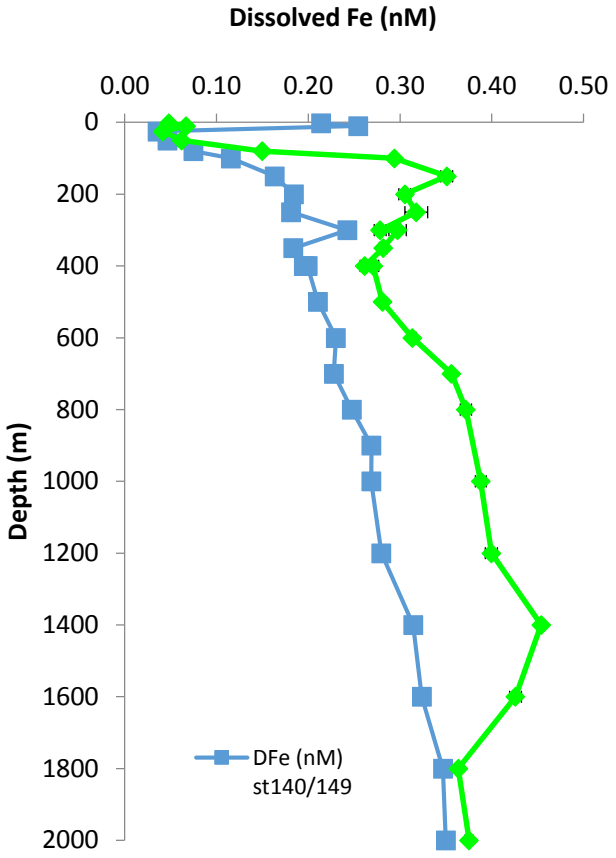

Figure 6.3. Profiles of dissolved iron against depth for stations 140 (blue, outside patch) and 150 (green, inside patch). Elevated DFe concentrations in Sta 150 from an unkown source may fuel the phytoplankton bloom.

Both profiles show low concentrations in the surface and increasing with depth. However, the station inside the bloom shows higher concentrations at depth all the way down to 1500 meters which might indicate a source of iron from below initiating this bloom. Although transmission data did not show evidence of particles in the water columns as an indication of hydrothermal input, this cannot be ruled out since the bloom was situated on a triple point where three large tectonic plates meet. The earthquakes in New Zealand prove that these contacts are active.

6.3.2 Objective 2: Organic complexation of Fe

The concentrations and binding strengths of the dissolved organic ligands will be used to explain the DFe concentrations with respect to the sources. Since the ligands determine the solubility of Fe they determine whether input from a source can remain dissolved and can be transported or will be scavenged or precipitated when the concentration is above the solubility of Fe in water.

All samples have been analyzed but the ligand characteristics have not yet been calculated except for a few stations. In general, it seems the concentrations of
dissolved organic ligands are relatively high in the polynya. The average concentration of dissolved organic ligands ([Lt]) over the whole water column in the polynya stations 20, 30 and 33 is 1.4 nEq of mol Fe, whereas the average [Lt] in the upper 300 m in the Eastern ACC (stations 1-10) is 0.84 nEq of mol Fe. Many samples in the polynya show the presence of two different dissolved organic ligands with different binding strength. Interestingly, this was not restricted to the surface layer but was also observed at depths of 300 m and deeper. The presence of multiple ligands is illustrated in the preliminary results of station 20 (Figure 6.4). Figure 6.4 shows the fit of the Langmuir model that describes reversible binding between Fe and the dissolved organic ligands in three different mathematical ways, non-linear (A) and two different linearized methods (B and C). Although the nonlinear fit in Fig 6.4A is superior, the two linear fits visualise the existence of two ligands by showing two linear parts formed by the data points instead of one linear part which is fitted by a line through these points. Calculating the characteristics of two ligands is complicated and will be done later.

In figure 6.5A the depth profile of DFe and ligand concentrations is shown for station 20, whereas figure 6.4B shows the ratio between [Lt] and DFe that represents the saturation of the ligands with Fe (Thuroczy et al 2011, 2012). The ratio is one when the ligands are saturated and greater than one when the ligands are unsaturated with Fe. Figure 6.5 shows that DFe in station 20 is very low, and only near the bottom (403m) the DFe increases. The ligand concentration is rather constant with depth near 1 nEq of M Fe. Near the bottom the ligands are saturated, thus the maximum DFe is reached.

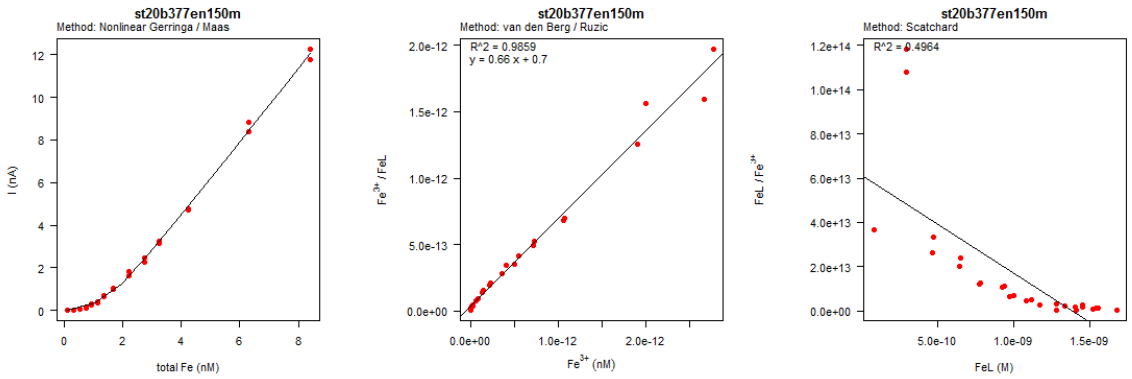

Figure 6.4. Three ways to fit the Langmuir model to describe organic complexation parameters assuming the existence of one ligand in sample 377 station 20, 150 m deep. The two right graphs are simplified linear models, they have the advantage that they show the existence of two ligands clearly by showing two linear parts in the data points. The middle graph shows in the low values a deviation from the linear model, whereas in the right hand graph the deviation from a linear model is even more clear, indicating the presence of two separate Fe binding organic ligands. Of course correct calculations will be applied later on in the data processing.

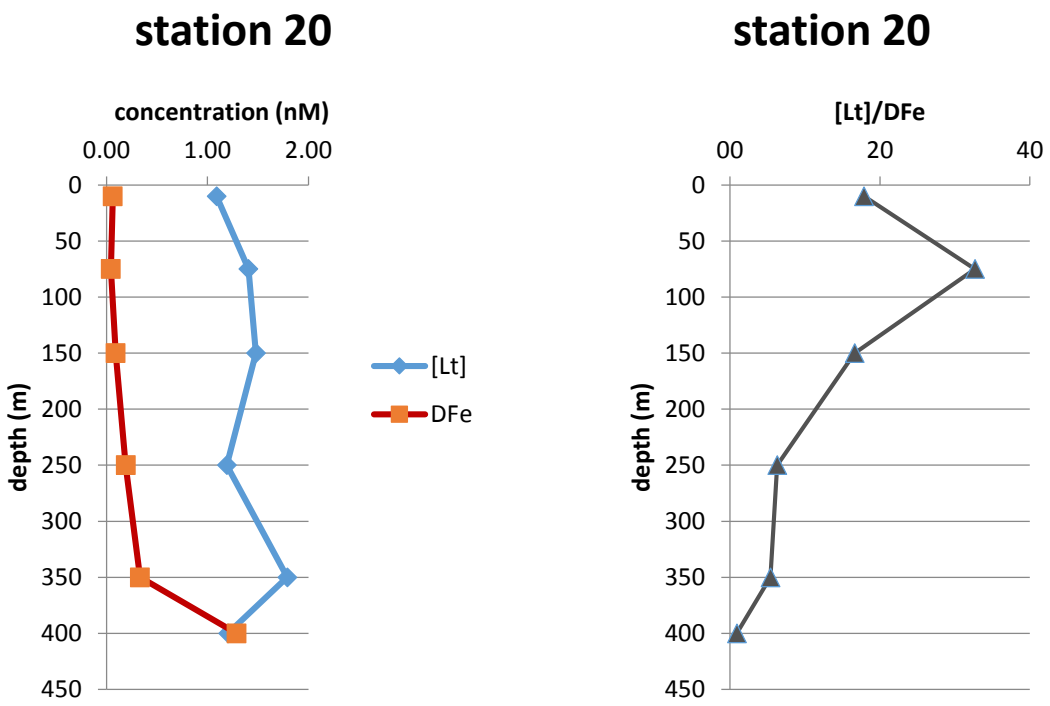

Figure 6.5. Ligand characteristics of station 20. A) DFe and organic ligand concnetrations with depth in station 20. B) the ratio between ligand concnetration [Lt] and DFe.

6.4 References:

Alderkamp, A-C, Mills, M.M, van Dijken, G.L., Laan, P., Thuróczy, C-E., Gerringa, L.J.A., de Baar, H.J.W., Payne, C., Tortell, P., Visser, R.J.W., Buma, A.G. J., Arrigo, K.R., 2012. Iron from melting glaciers fuels phytoplankton blooms in Amundsen Sea (Southern Ocean); phytoplankton characteristics and productivity. DSR II, 71-76, 32-48.

Arrigo, K. R. , D. L. Worthen, D. H. Robinson, 2003. A coupled ocean-ecosystem model of the Ross Sea: 2. Iron regulation of phytoplankton taxonomic variability and primary production. *J. Geophys. Res*. 108, No. C7, 3231, doi:10.1029/2001JC000856

de Baar, H.J.W., Buma, A.G.J., Nolting, R.F., Cadee, G.C., Jacques, G., Tréguer, P.J., 1990. On iron limitation of the Southern Ocean: experimental observations in the Weddell and Scotia Seas. Mar. Ecol. Progress Ser. 65, 105–122.

de Baar, H.J.W., de Jong, J.T.M., Bakker, D.C.E., Löscher, B.M., Veth, C., Bathmann, U., Smetacek, V., 1995. Importance of iron for phytoplankton spring blooms and CO2 drawdown in the Southern Ocean. Nature 373, 412–415.

de Baar, H,.J.W. et al., 2005. Synthesis of iron fertilization experiments: From the Iron Age in the Age of Enlightenment. Journal of Geophysical Research, 110.

Coale, K. H., et al., 1996. A massive phytoplankton bloom induced by an ecosystem-scale iron fertilisation experiment in the equatorial Pacific Ocean, Nature, 383, 495– 501.

Croot P.L., Johanson M. (2000). Determination of iron speciation by cathodic stripping voltammetry in seawater using the competing ligand 2-(2-Thiazolylazo)-p-cresol (TAC). Electroanalysis. 12, No.8, 565-576.

Gerringa, L.J.A.; Herman, P.M.J.; Poortvliet, T.C.W. (1995). Comparison of the linear Van den Berg / Ruzic transformation and a non-linear fit of the Langmuir isotherm applied to Cu speciation data in the estuarine environment. Marine Chemistry. 48, 131-142.

Gerringa, L.J.A, Alderkamp, A.-C, Laan, P, Thuróczy, C-E, de Baar, H.J.W., Mills, MM, van Dijken, G.L., van Haren, H., Arrigo, K.R., 2012 Iron from melting glaciers fuels the phytoplankton blooms in Amundsen Sea (Southern Ocean); iron biogeochemistry. DSR II, 71-76, 16-31.

Gerringa, L.J.A., Rijkenberg, M.J.A., Thuróczy, C.-E., Maas, L.R.M. (2014) A critical look at the calculation of the binding characteristics of Fe binding organic ligands, Environmental Chemistry, in press

Gledhill, M. and van den Berg, C.M.G., 1994. Determination of complexation of iron (III) with natural organic complexing ligands in seawater using cathodic stripping voltammetry. Mar. Chem., 47: 41-54.

Johnson et al., 2007. Developing standards for dissolved iron in Seawater. Eos, Vol 88, n. 11.

Johnson, K.S., R. M Gordon, K. H. Coale, 1997. What controls dissolved iron concentrations in the world ocean? Marine Chemistry 57, 137-161

Klunder, M. B., Laan, P., Middag, R., de Baar, H. J. W., and van Ooijen, J. C. (2011) Dissolved Fe in the Southern Ocean (Atlantic sector), Deep-Sea Res. Pt. II, 58, 2678–2694.

Martin, J.H., et al., 1994 . Testing the iron hypothesis in ecosystems of the equatorial Pacific Ocean. Nature 371, 123–129.

Sedwick, P. N, Marsay, C.M., Sohst, B.M., Aguilar-Islas, A.M., Lohan, M.C., Long, M.C., Arrigo, K.R., Dunbar, R.B., Saito, M.A., Smith, W.O., Di Tullio, G.R., 2011. Early season depletion of dissolved iron in the Ross Sea polynya: Implications for iron dynamics on the Antarctic continental shelf, J. Geophys. Res., 116, C12019,

Thuróczy, C.-E., Gerringa, L., Klunder, M., Laan, P., de Baar, H., 2011. Observation of consistent trends in the organic complexation of dissolved iron in the Atlantic sector of the Southern Ocean. Deep-Sea Res. II 58, 2695–2706.

Thuróczy, C-E, Alderkamp, A.-C. Laan, P, Gerringa, L.J.A., de Baar H.J.W., Arrigo, K.R., 2012. Key role of organic complexation of iron in sustaining phytoplankton blooms in the Pine Island and Amundsen Polynyas (Southern Ocean). DSR II, 71-76, 49-60.

7. Genetic characterization of *Phaeocystis antarctica*

Tom Delmont and Anton F. Post (not on board)

Phaeocystis antarctica is a photosynthetic phytoplankton species that has evolved in the cold waters of the Southern Ocean. It shows at least two different morphotypes; flagellated single cells and spherical colonies that are thought to be protected from grazing. *P. antarctica* regularly outperforms diatoms and other photosynthetic alga in several Antarctica polynyas (and as encountered during this cruise, also in the Antarctica circumpolar current) where they form dense phytoplankton blooms and influence the cycles of carbon and sulfur. But yet, little is known on the genetic diversity and functionality of this photosynthetic alga in the Southern Ocean, limiting our ability predicting its acclimation responses when confronted to environmental variations. Interestingly, the recent emergence of efficient sequencing technologies provide new opportunities to characterize the genomic content of the alga and to quantify population diversity in the Southern Ocean based on genetic structure variations. Moreover, it is now possible to deeply sequence RNA molecules extracted directly from the environment, therefore permitting the connection of expressed *P. antarctica* genes (i.e., those encoding proteins in a given condition) and key environmental conditions. However, *P. antarctica* gene content has first to be characterize using pure cultures. Consequently, researchers from the Marine Biological Laboratory (Tom Delmont and Anton Post) and Stanford University (Anne-Carlijn Alderkamp and Kevin Arrigo) recently accomplished a comprehensive functional assessment of a well described *P. antarctica* strain using a multi-library transcriptomic sequencing strategy

by varying light and iron availability (manuscript in progress). This controlled laboratory experiment resulted in the detection and partial functional identification of more than 25 000 transcripts. Interestingly, both physiological observations and transcriptomic data indicated a clear switch from colonies to single cells under nutrient limitation. Moreover, the *P. antarctica* transcriptomes were highly dissimilar between the two states, with more than 8 000 differentially expressed transcripts. These transcriptomic datasets provided critical information regarding functional activity differences between single cells and colonies (e.g., mobility, cytoskeleton, homeostasis, nutrients acquisition) in addition to the direct response of the alga to iron availability (e.g., heme production under Fe-replete conditions, iron transporters and ferrichrome iron receptors under Fe-limitation). Finally, these transcriptomic data revealed that iron limited single cells and iron repleted colonies have different functional activity responses (in addition to a core response) to light intensity variation, emphasizing complex genetic mechanisms behind *P. antarctica* light acclimation. Thanks to this achievement, it is now possible to map metatranscriptomic data generated directly from the environment (i.e., transcriptomic data representing more than one taxonomical group) to this newly described alga transcriptome, rending possible the quantification of expressed genes within the *P. antarctica* natural populations evolving in the Southern Ocean. These *in situ* functional investigations are essential to support *in lab* observations and will build on those observations to provide new information regarding 1) functional acclimation mechanisms of *P. antarctica*, 2) *in situ* life style (single cells vs colonies), and 3) genetic diversity between *P. antarctica* populations in different environments (e.g. low biomass regions such as the Antarctic Circumpolar Current and high biomass regions such as the Ross Sea polynya) and 4) functional diversity between *P. antarctica* populations in different environments.

7.1 Objectives

7.1.1 Aim 1. Investigating P. antarctica functional activity through gene expression.

Our principal aim was to investigate for the first time gene expressions within natural populations of *P. antarctica* natural populations in the Ross Sea polynya (during the austral summer bloom event of 2013-2014) and in different locations of the Antarctica Circumpolar Current. We first sampled biological material to study the natural functional state of the alga in different depths and locations of the Southern Ocean. Secondly, we sampled the bioassay experiments described in section XX to investigate the gene expression response of *P. antarctica* natural populations to varying light intensities and iron concentrations. Finally, we collected samples to separately study the functional activity of *P. antarctica* single cells (2-10µm fraction) and colonies (10-105µm and >105 µm fractions) using a size fractionation strategy.

7.1.2 Aim 2: Investigating P. antarctica phenotypic and genetic diversity

The second aim of the project was to investigate the diversity of *P. antarctica* populations in the Southern Ocean. Both phenotypic criteria and genetic markers can be used to observe differences within these populations. For the phenotypic investigation, the main objective was to characterize the physical aspects of *P. antarctica* colonies (size, number of cells per colony, *etc.*) directly from the vessel. Therefore, the shape of *P. antarctica* colonies and organization of cells within these structures were described in both the Antarctica Circumpolar Current and the Ross Sea polynya (low versus high activity areas) using a dissecting microscope (see figure 7.1 for a selection of *P. antarctica* colony images). Moreover, samples dedicated to the sequencing of genetic markers (e.g., 16S/18S rRNA gene amplicon datasets) and metagenomes (i.e., all genetic structures present in a given sample) were collected to investigate the genetic diversity of *P. antarctica* in the surface and deeper layers of key areas of the Southern Ocean. Finally, the metatranscriptomic datasets (see "Aim 1" section) can also be used to quantify genetic variations of expressed genes within *P. antarctica* populations, providing additional information regarding their diversity.

7.1.3. Aim 3: Investigating bacterial communities associated with P. antarctica colonies

We recently discovered that specialized heterotrophic bacterial taxa associated preferentially with the alga in an Antarctica polynya (Amundsen Sea, West Antarctica). The investigation of their genomic content highlighted several functional mechanisms that have the potential to directly influence the primary productivity of the alga (e.g., cobalamin production). However, additional investigations are required to fully understand their interactions with the alga. Therefore, in addition to the genetic investigations of *P. antarctica* natural populations (see "Aim 1" and "Aim 2" sections), our third and last aim during this cruise was to study the diversity and functionality of bacterial communities when associated to (and possibly infecting and/or degrading biomass from) *P. antarctica* colonies in the Ross Sea polynya and Antarctica circumpolar current. One of the main objectives was to investigate their functional activity when attached to the alga and to define key functional mechanisms directly related to the alga metabolism.

7.2 Methods and sample collection

Throughout sample collection for metatranscriptomic analysis a particular effort was made to collect biological samples in a limited period of time in order to study the *in situ* activity of the alga and prevent changes due to responses to sampling conditions as much as possible.

7.2.1 Phytoplankton sampling for metatranscriptomic datasets (aim 1)

- *Core sampling (113 samples)* –Phytoplankton biomass was collected from one to four depths from all core stations (see section 4). Depending on the biomass, we filtered 0.7-4.0 L onto 0.2 µm filters that were flash frozen in liquid nitrogen and stored at -80°C. Sampling time from collecting samples from the CTD to flash freezing was approximately 30 min.
- *Bioassay experiments (252 samples)*
    - **Ross Sea:** Four experiments performed by varying light and iron availability (see section 3).
    - **Antarctic circumpolar current bloom:** Five experiments (iron availability only, see section 3).
    - **Sampling strategy:** From each of the treatments phytoplankton biomass was sampled from the triplicate incubation bottles, filtered onto 3µm filters, flash frozen in liquid nitrogen and stored at -80°C. Sample volumes were 0.15 L and 2.2 L depending on biomass and less than 15 min was required from sampling to flash freezing.

7.2.2 Size fractionation to disjointedly acquire DNA and RNA from P. antarctica single cells and colonies (aim 1)

Phytoplankton biomass was collected in different size fractions of >105µm (enriched in *P. antarctica* colonies), 2-105µm (enriched in *P. antarctica* single cells, small colonies and diatoms) and <2µm (enriched in bacteria). In the Ross Sea Polynya samples were collected at 10 and 200 meters depth (36 samples total), and in the Antarctic Circumpolar Current bloom at 10 meters depth (38 samples).

7.2.3 Sampling for phytoplankton community structure in order to generate 16S/18S rRNA gene amplicons and metagenomic datasets (aim 2)

Phytoplankton biomass was collected from surface waters using the in line water system of the Nathaniel B. Palmer. 0.5 L to 20 L of seawater was filtered onto 0.2 µm filters (87 samples). Moreover, samples from

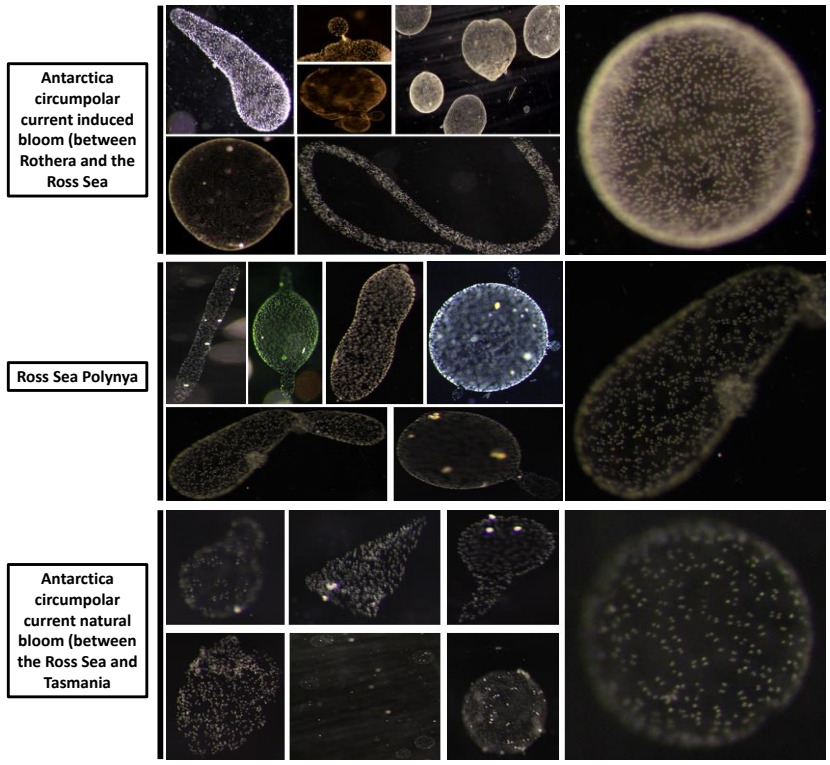

Figure 7.1. Images of *P. antarctica* colonies isolated from the Ross Sea polynya and Antarctica Circumpolar Current (ACC) under a dissecting microscope. Colonies from the Ross Sea were isolated directly from surface waters, whereas colonies from the ACC grew after incubation for several weeks. The scale of the different images varies depending on the size of the colony.

deep waters were collected in the Ross Sea Polynya from 200 to 700 m depth by filtering 4L- to 8L of seawater onto 0.2 µm filters.

7.2.4 P. antarctica colonies surface colonization, infection and/or biodegradation by bacterial communities sampled from the euphotic zone and below the euphotic layer (90 samples) (Aim 3):

To investigate the bacterial communities that may be associated with *P. antarctica blooms* we conducted a bioassay experiment in which we incubated colonial *P. antarctica* from the Ross Sea with different bacterial populations. For these experiments 100L of surface water from the Ross Sea was filtered at 105µm. The >105µm fraction was re-suspended in 1L of filtered water (from the surface) and inoculated with i) filtered water (<0.2 µm, no bacteria) (3 bottles), ii) bacteria (0.2-2µm size fraction) sampled from the surface + filtrated water (3 bottles), and iii) bacteria (0.2-2µm size fraction) sampled from bellow 300m depth (expected to be efficient at degrading *P. antarctica* biomass) + filtrated water (3 bottles). Experiments were run over 25 days and each treatment was sampled every 5 days by filtering 150 ml sample using size fractionation of >10µm to study bacteria attached to *P. antarctica* colonies and 0.2-10µm to study free living bacteria.

7.3 Preliminary results

7.3.1 Analysis of P. antarctica colonies (aim 2)

While most of our scientific analyses will be performed at the Marine Biological Laboratory (especially, DNA and RNA extraction, 16S/18S rRNA, metagenomic and metatranscriptomic library constructions, high throughput sequencing, bioinformatics analysis), a few preliminary results are already available. It is in particular the case of microscopy observations of new *P. antarctica* colony shapes not previously described (see Fig 7.1 for a selection of representative phenotypes). Especially, we observed colony division events, a phenotypic characteristic that has been described for *P. pouchetii*, the *Phaeocystis* species in high latitudes of the northern hemisphere. However, to our knowledge, colony division has not been described for *P. antarctica*. Moreover, cell organization within *P. antarctica* colonies was different between colonies isolated after incubation of Antarctica circumpolar current waters (evenly distributed, dense), and colonies

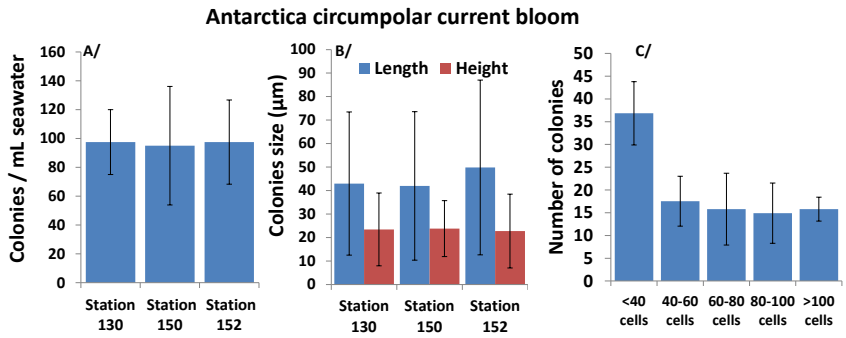

Figure 7.2 A) number of *P. antarctica* colony per milliliter of sea water, B) colony size and C) number of cells per colony estimated from three stations in the Antarctica circumpolar current bloom. These estimations are based on the sampling of 20L of Seawater from the surface (10m depth), followed by the analysis of 8 sub-samples of 50µL per station using a dissecting microscope.

isolated from the Ross Sea (organized in groups of two or four cells). This observation suggests either a strong acclimation response of the same organism to environmental variations between the different regions or the existence of different taxonomical groups.

Microscopic analysis of *P. antarctica* colonies from the ACC bloom revealed some interesting characteristics. The population density and size of *P. antarctica* colonies were quantified in three locations of this bloom (Fig. 7.2). Based on this microscopy work, key water parameters (especially, mixed layer depth and fluorescence intensity) and satellite data (to estimate the spatial extent of the bloom), we provide a preliminary estimation number of 10^{19} *P. antarctica* colonies evolving in this localized area of the Southern Ocean (estimation based on a number of 10^{8}colonies/m^3 in the first 30 meters of an area of 200km of length and 100km of height). The length and height of these colonies were in the order of 40µm and 20µm respectively, substantially smaller than those observed in the Ross Sea (data not shown). Moreover, most of the colonies were hosting less than 100 *P. antarctica* single cells. These estimations will be adjusted in the coming weeks based in part on high throughput microscopic imaging generated from the FlowCam in different depths of the bloom, but already emphasize the importance of this biological hotspot and the scientific interest of the biological samples collected from this area.

Surprisingly, a substantial fraction of the colonies in this bloom were hosting one to several free living cells (in addition to *P. antarctica* cells). Photo and video observations showed that these cells were significantly larger than the *P. antarctica* colony cells (diameter approximately 10 times bigger than *P. antarctica* cells) and exhibited motility within the colonies, a phenotypic characteristic not observed in *P. antarctica* cells. To our knowledge, these cells have not been observed before within *P. antarctica* colonies. These microorganisms have yet to be characterized but might represent grazers feeding on *P. antarctica* cells from within colonies or symbionts enhancing *P. antarctica* activity. Finally, the *P. antarctica* colony phenotypic diversity observed between the Antarctica circumpolar current and the Ross Sea polynya was unexpected (Fig 7.1) and strongly suggests these phytoplankton populations possess a taxonomical and functional diversity higher than expected. These exiting preliminary findings will soon be reinforced by the *P. antarctica* genetic investigations (both taxonomical and functional) that will be performed in the coming months at the Marine Biological Laboratory and University of Stanford.

8. Isolation of phytoplankton cells for future physiological experiments and reference transcriptome datasets

Bethany Jenkins – University of Rhode Island

8.1 Isolation of diatoms

Cells were isolated from underway samples collected in the Drake Passage enroute to the Antarctic Peninsula and from daily trace metal or conventional CTD casts. Cells were concentrated over gravity filtration over a 5µm mesh PVC cell concentrator. In low biomass waters >1.5 µg chlorophyll fluorescence 4-8 L were typically concentrated to ~ 50 mls and in higher biomass waters 2 L of water was concentrated to ~ 50 mls. Phytoplankton community composition in the concentrated underway samples was determined by Hannah Joy Warren using the FlowCam. Once CTD deployments began, cells were concentrated from water collected at 10 m in either the trace metal CTD rosette or more typically from the conventional CTD that was deployed in parallel following daily trace metal CTD casts. Concentrated biomass was visualized using a dissecting microscope to capture an overall sense of cell density and community composition. One tenth of the total concentrate was used to inoculate culture media. Representative individual cells from each station were isolated into culture by pipetting and rinsing the cells in filtered sea water. Rinsed cells were used to inoculate media in 48 well culture plates. Media for initial isolations consisted of filtered surface sea water amended with F/2 nutrients, trace metals and vitamins. Plates and cell concentrate were incubated in a Percival incubator set to 0.3 ˚C and 33 µEinsteins/m2/sec light at a 14 hr light/6 hr dark cycle. Growth was followed in the plates using the dissecting microscope. After several weeks it was determined that the nutrient regimes (particularly the trace metals) in the media might too high given in situ iron concentrations and isolations after 12/22/13 were done with filtered sea water amended with F/20 tracemetal and vitamin additions only. Overall growth was more robust in the F/20 media but this was also impacted by an adjustment to onboard Percival incubator that had a bulb go out.

Diatoms communities in the Drake Passage and low biomass stations were dominated by *Corethron spp*., *Thalassiothrix spp*., *Proboscia spp*. and also several single celled centric diatoms that varied in size. The presence of chain forming diatoms such as *Chaetoceros spp*. and *Eucampia spp*. began to be detected at -64.4560 N -68.3755 W and were present in the majority of stations sampled in the Ross Sea. Due to a large growing database of genomic and transcriptomic information for Thalassiosiroids in the Jenkins laboratory, particular effort was directed at isolated representatives of this genus. More specifically, isolates of *Thalassiosira rotula*, *T. gravida, T. antarctica* and *T. auguste lineat*a were desired and a particular focus. These will serve for comparative physiological experiments in the Jenkins laboratory as well as for comparative transcriptomics with temperate isolates of the same species for which we have transcriptome data (e.g. *T. rotula*). Chain forming Thalassiosiroids were not detected at many locations, but were present and isolated from stations 18, 19, 75, 92 and 101.

Overall, isolation was attempted for 624 cells and a success rate of 33% growth for the isolates was obtained in the 48 well plates. Fortunately, the isolation and growth of chain forming *Thalassiosiroids* was particularly successful, as was growth of large single celled centrics such as *Coscinodiscus spp*. Isolation attempts for *Corethron* and *Thalassiothrix* spp. were not successful, but Corethron persist in cultures inoculated from concentrated cells. Isolates and cultures will be transported back to the Jenkins laboratory for propagation and future physiological and transcriptome analaysis.

8.2. Isolation of Phaeocystis cells

At Ross Sea (91,101,113and 120) and ACC bloom stations (135,152) where large *Phaeocystis* colonies were observed, biomass was concentrated by gravity over 105 µm filters and rinsed into sterile seawater enriched with F/20 vitamins and nutrients. Cultures were also inoculated with colonies from Fe addition

experiment 1. Enriched *Phaeocystis* cultures will be transported to the Arrigo and Jenkins laboratories for future physiological experimentation and genotyping of the *Phaeocystis* isolated at different locations.

8.3. Filtration of Samples for Diatom DNA and RNA analysis

Jenkins has developed high throughput methods to compare diatom community composition (Chappell et al 2013) and sensitive molecular markers for diatom iron limitation. One of her major goals in participating in this cruise was to collect samples for genetic analysis of diatom community composition and to develop markers of Fe status in Antarctic diatom species. At underway stations through the Drake Passage and at each CTD where water was collected, biomass was filtered for DNA and RNA samples using a masterflex peristaltic pump with the washdown controller set at 3. Triplicate RNA and DNA samples were filtered at each depth determined for P vs. E curves (two depths per cast). Typically, in all but the highest *Phaeocystis* biomass stations, samples were filtered onto 0.2 µm 25 mm Supor filters. In general, 1.5-2 L was filtered, sufficient biomass for down stream analysis. At stations with very high *Phaeocystis* biomass, it was necessary to size fractionate samples in order to obtain enough biomass on the filters. In those instances, a 10 µm 25 mm polyester filter was placed upstream of the 0.2 µm Supor filter and biomass was captured on both. At the high *Phaeocystis* biomass stations often it was only possible to filter 350 ml of water onto the 0.2 µm filter even when the 10 µm prefilter was placed upstream.

Samples were also collected for future work aimed at bacteria that might degrade freshly exported phytoplankton biomass. At each trace metal cast where water was collected for core measurements, duplicate 2 L samples from 200 meters were filtered onto 0.2 µm Supor filters. In total, 960 RNA and DNA samples were collected.

8.4. References

Chappell, P. D., L. Whitney, T. L. Haddock, S. Menden-Deuer, E. G. Roy, M. Wells, and B. D. Jenkins. Thalassiosira spp. Community Compostion Shifts in Response to Chemical and Physical Forcing in the Northeast Pacific Ocean Frontiers in Aquatic Microbiology,. 23 September (2013)

Whitney, L.P., Lins, J.J., Hughes, M.P., Wells, M.L., Chappell, P.D., and Jenkins, B.D. Characterization of putative iron responsive genes as species-specific indicators of iron stress in Thalassiosiroid diatoms. Frontiers in Aquatic Microbiology 25 November (2011)

9. Small scale physical context

Kate Lowry and Leif Thomas (not on board) – Stanford University

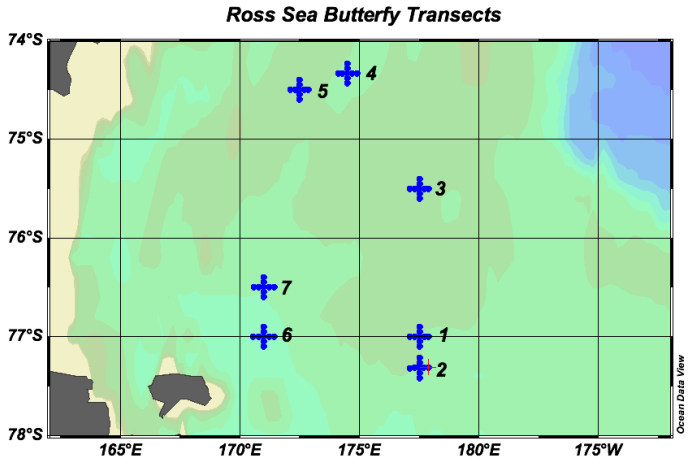

Figure 9.1. Locations of butterfly transects in the Ross Sea Polynya.

'Butterfly' transects were conducted around some of the 'daily' biological stations to characterize the physical environment that influences phytoplankton distributions and spatial variability. The butterfly consisted of two perpendicular transects (north to south and east to west) with stations spaced 3 nautical miles (~5.6 kilometers) apart for a total of nine CTD sensor profiles, including a final cast approximately 10 hours later at

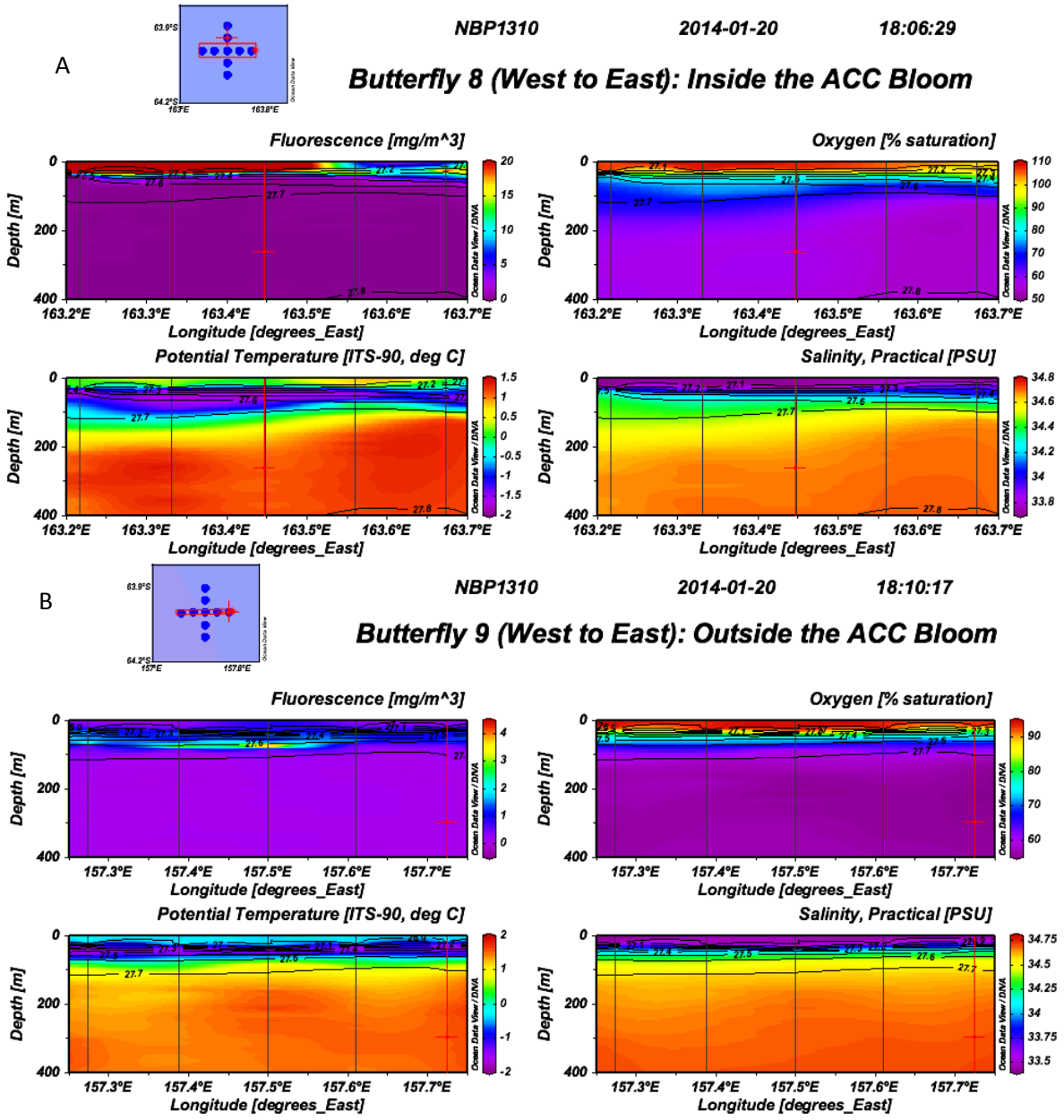

Figure 9.2. Examples of two butterfly transects in the ACC, A) inside the phytoplankton bloom and B) outside the bloom

the starting location to assess temporal variability. Data available during the butterfly include the CTD sensors (salinity, temperature, oxygen, fluorescence, beam transmission, PAR, and sound velocity) as well underway data (e.g. temperature, salinity, oxygen, fluorescence, pCO_2, transmission, currents via ADCP, bathymetry, etc.), meteorological data (e.g. winds, air temperature, barometric pressure, surface PAR), and the MIMS data.

Over the course of the cruise we conducted nine butterflies, with seven in the Ross Sea Polynya and two in the ACC. Of the butterflies in the Ross Sea (Fig 9.1), four of the butterflies were at the locations of our bioassay experiments (1,2,6,7), one was at a location dominated by diatoms (3), one was in a deep trough (4), and one was on a shallower bank (5). Of the two ACC butterflies, one was inside the bloom (8) and one was outside the bloom (9). The goal of conducting butterflies surrounding experiment sites was to

provide context for the physical environment of the phytoplankton that we are studying with the bioassay experiments, while the additional butterflies were conducted to provide information about the spatial variability of the physical and biological environment in areas with blooms of *P. antarctica* and/or diatoms and in areas without phytoplankton blooms.

Fig 9.2 provides an example of how the butterfly data can be used to characterize the physical environment surrounding a 'daily' station and to compare and contrast two different environments. Fig 9.2a shows fluorescence, oxygen, potential temperature, and salinity data for the west to east transect inside the ACC bloom, while Fig 9.2b displays the same data for the west to east transect at the same latitude but outside the bloom.

10. Dimethylsulfide dynamics

Casey Schine, Laughlin Barker, John Dacey (not on board), Philippe Tortell (not on board)

Dimethylsulfide (DMS) is a volatile reduced sulfur compound produced by phytoplankton and bacteria. DMS diffuses from ocean surface waters into the atmosphere, where it is rapidly oxidized to form sulfate aerosols that influence regional albedo. The annual radiative forcing resulting from DMS emissions from the global oceans has been estimated at -2 W m^{-2} (Thomas *et al.*, 2010). In

the Southern Hemisphere where anthropogenic sulfate emissions are low and ocean area is high, DMS plays a substantial role in the production of atmospheric sulfate, contributing as much as 43% of the annual atmospheric sulfur burden, and the estimated radiative forcing over the Southern Ocean during the austral summer from oceanic DMS emissions is -9.32 W m^{-2}. The Ross Sea has some of the highest recorded concentrations of DMS, with an average concentration of 32 nM, compared to the Southern Ocean and global averages of 11 nM and 4 nM, respectively. Seawater concentrations of DMS result from numerous production and consumption processes within the marine ecosystem involving the activity of phytoplankton, zooplankton, and bacteria. Understanding why the balance of these processes results in anomalously high DMS concentrations in the Ross Sea will help us to understand how DMS emissions in this region may be affected by climate change.

10.1 MIMS underway measurements.

On this cruise, we measured real-time underway concentrations of the biogenic gases CO_2, O_2/Ar, N_2/Ar and dimethylsulfide (DMS) using membrane-inlet mass spectrometry (MIMS). The MIMS system is provided seawater through the ship's underway system, and records GPS-provided time-stamps and position. The system automatically cycles through a single seawater standard every 30 minutes, while a more complete set of CO_2 and DMS standards were run twice daily when on station.

The distributions of gases along the full cruise track are shown in several figures. During our southbound transit along the Antarctic Peninsula to Rothera Station we observed relatively uniform surface water gas concentrations with the exception of a small patch of elevated Chl *a* concentrations indicative of high surface productivity, accompanied by relatively high DMS concentrations at approximately 62.5 S (November 23, 2013). During our western transit to the Ross Sea from Rothera Station (along 65 S latitude), DMS concentrations and biological productivity remained low. Once in the ice and continuing into the polynya, we observed dramatic changes in all gases on very small time and spatial scales. pCO_2 concentrations ranged from approximately 200 to 400 ppm, with the lowest values corresponding to the initial *P. antarctica* bloom discovered in eastern portion of the polynya. O_2/Ar and CO_2 were strongly anti-correlated throughout the study area, indicating that biological activity rather than physical effects exerted a dominant control on CO_2 and O_2 distributions in this region. DMS concentrations in the polynya were patchy and highly variable, with high concentrations strongly correlated with *P. Antarctica*-dominated waters (as determined by FlowCam analysis of the sampled waters). Peak underway DMS concentrations inside the polynya were approximately 40 nM. Exiting the polynya, DMS spiked and O_2/Ar and CO_2 rose

and fell respectively, indicating high surface productivity near the ice edge. During our northern transit, exiting the Ross Sea and heading towards Hobart, Tasmania, we encountered a *Phaeocystis*-dominated phytoplankton bloom in the ACC. Underway DMS concentrations (Fig 10.1) inside the bloom were consistently over 100 nM (2x higher than the highest concentrations seen in the polynya). Underway DMS measurements provided a high-resolution spatial map of the bloom's extent, and the relationship between DMS, pCO_2 and ΔO_2 /Ar.

10.2 DMS/P/O discrete concentration measurements.

DMS, dimethylsulfoniopropionate (DMSP), and dimethylsulfoxide (DMSO) concentrations were measured at 49 different stations with 2 depths measured at each station, and on 10 separate bioassay experiments. Duplicate bottles for DMS/P/O samples were collected directly from the GoFlo bottles and filled to overflowing to minimize headspace volume and the potential for DMS loss. Bottles were then stored in the dark under ambient seawater temperatures until analysis (< 1h).

Triplicate DMS samples were measured immediately by gently syringe filtering (through a GF/F filter with a nominal pore size of 0.7 μm) 10-20 ml through a GF/F filter into a 60 ml amber glass serum vial with a Teflon-coated butyl rubber stopper. Samples were then connected to a 16-position manifold valve and sequentially sparged with nitrogen gas for 10 min and concentrated on a Carbopak-X trap at room temperature. Upon completion of sparging the trap was heated to ~250°C to desorb the DMS, which was then carried through a Chromasil 330 packed column, before detection by a quadropole mass

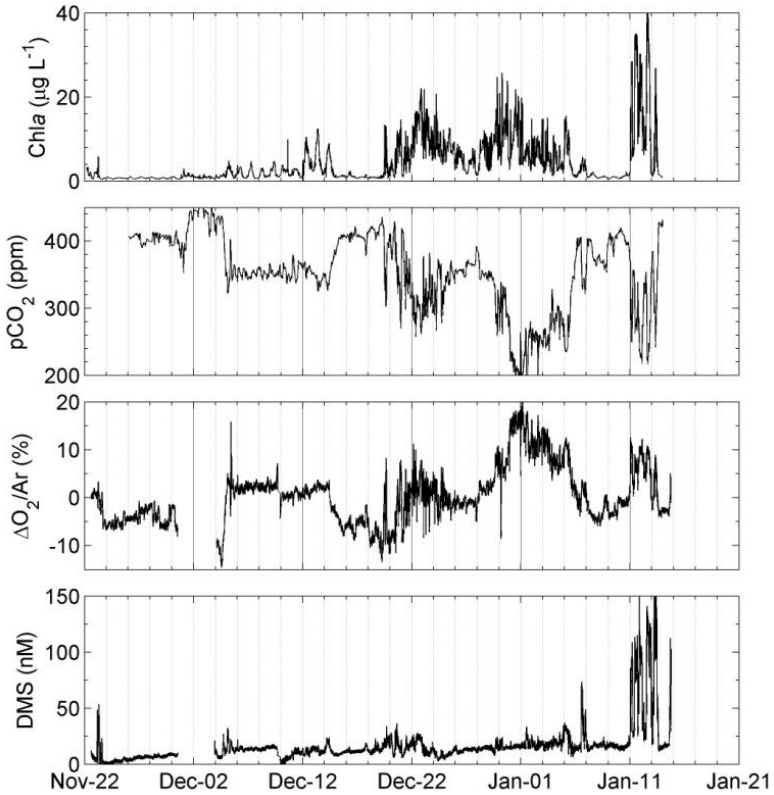

Figure 10.1. Underway data showing Chl*a* and pCO_2 (from ship's underway systems) and ΔO_2 /Ar ratio and DMS concentrations provided by the MIMS system.

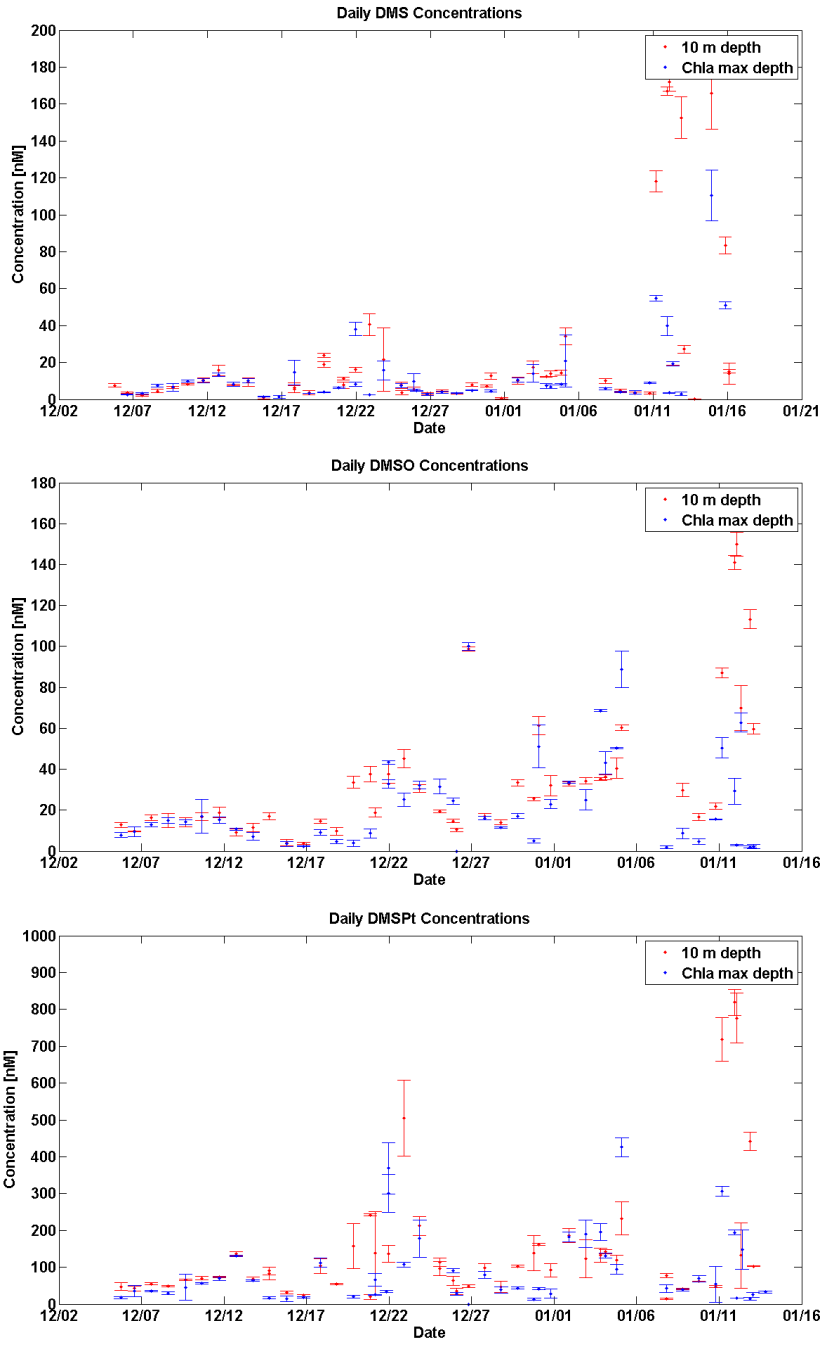

Figure 10.2 Discrete concentration measurements made on PT-CIMS of DMS, DMSO, and DMSPt (DMSPd+DMSPp+DMS).

Dissolved DMSP (DMSPd) samples were collected by amending DMS samples (after analysis for DMS) with NaOH (to a final concentration of 1N), to generate DMS from DMSP hydrolysis, and stored for a minimum of 48 h before analysis. The contents of each vial were then analyzed for DMS on the PT-CIMS.

Unfiltered water samples (10 ml) for total DMSP (DMSPt) concentration were pipetted into a gas tight vial. Triplicate samples from each depth were immediately treated with NaOH (for a final concentration of

1N), to generate DMS from DMSP hydrolysis, and stored for a minimum of 48 h before analysis. The contents of each vial were analyzed for DMS using the PT-CIMS. Particulate DMSP (DMSPp) concentrations will be calculated by subtracting the DMS and DMSPd concentrations from DMSPt concentration (this work has not been done yet, and so DMSPt concentrations are reported here).

Samples for dissolved DMSO (DMSOd), in triplicate, were collected by syringe filtering 20 ml of water through a GF/F filter. Filtrate was collected in an amber serum vial and then immediately sparged with nitrogen to remove endogenous DMS. Samples were then treated with $TiCl_3$ to quantitatively reduce DMSO to DMS at a ratio of 1:1 (Kiene and Gerard, 1994). Samples were stored a minimum of 48 h before being analyzed for DMS on the PT-CIMS. An in-line trap of Na_2CO_3 was added upstream of the trapping system to prevent acid vapors from reaching the gas chromatograph.

Preliminary results showed three patches of elevated DMS concentrations (Fig 10.2), along with elevated DMSO and DMSPt concentrations. The first patch (starting Dec 19th) corresponds with the *Phaeocystis*-dominated waters sampled in the Ross Sea polynya. The second patch (starting December 31st) is of slightly lower magnitude than the first high DMS patch and corresponds with our return to the same location as the first patch. This second patch of high DMS concentrations, however, is more apparent in DMSPt and DMSO concentrations than in DMS concentrations. The third patch (starting around January 11th) corresponds with the ACC bloom. DMS concentrations in the ACC bloom were more than 5 times those in the Ross Sea. An interesting, but still preliminary, finding is that the DMSPt concentrations showed an increase of much smaller magnitude than DMS concentrations between the Ross Sea and the ACC bloom. It will be interesting to investigate how similar pools of particulate DMSP (the pool that drives DMSPt concentrations) yield such different accumulations of DMS.

12.3 DMS production/consumption rate measurements.

DMS rate measurements were taken at a single depth (10m) at 16 different stations. Water was collected from the CTD and stored in a cubitainer at 4°C. Quadruplicate samples (2L each) were transferred into UV transparent, gas tight, Welch Fluorocarbon 0.005" PFA bags with no headspace. Each bag was then amended with $^{2}H_3$-DMS, $^{2}H_6$-DMSPd, and $^{13}C_2$-DMSOd to ~10% of ambient concentrations. Bags were then incubated in deckboard incubators at 30% of incident irradiance. Bags were subsampled every 2-3 hours over the course of 6-8 hours. DMS produced from DMSP and DMSO was analyzed as described above, and concentrations of different isotopically labeled species were measured by peak jumping between m/z 62, 64, 65, and 68 (48 was sometimes used in place of 64). Four DMS samples were collected at each time point (1 from each bag) and 2 of these samples were analyzed for DMSPd and 2 were analyzed for DMSOd following DMS measurement. Tracer production and consumption rates will be calculated using linear regression of average concentrations (of 4 replicate bags) over 3 timepoints.

11. Phytoplankton photoinhibition - Surface Irradiance Exposure

Anne-Carlijn Alderkamp

Phytoplankton residing in the upper mixed layer of the water column receive a variable light climate due to seasonal and dial light cycles, changes in ice and cloud cover, and wind driven vertical mixing of the watercolumn. These alterations require acclimation of light harvesting and protective mechanisms to ensure maximum photosynthetic efficiency at low light levels and protection from photoinhibition at high light levels. The objective of the NBP13-10 cruise is to determine 1) if Antarctic phytoplankton experience photoinhibition when residing near te surface, 2) differences in photoinhibition characteristics between sea

ice, polynya, and open ocean phytoplankton, and 3) the importance of repair of photodamage versus photoprotection.

11.1 Work at sea

Short term deck incubations were caried out at 5 stations in the sea ice zone (SIZ) before entering the Ross Sea Polynya, 4 stations in the Ross Sea Polynya, and 1 station north of the SIZ, as described in Alderkamp et al (2010, 2011, 2012). Samples contaning *in situ* phytoplankton were collected from surface water and the chlorophyll maximum. The maximum efficiency of photosystem II (PSII) (Fv/Fm) was analyzed with a PAM fluorometer. Samples were incubated for 20 mins at incident light levels in transparent deck incubators. The decrease in photosynthetic efficiency of the phytoplankton was determined by PAM fluorometer. Subsequently, recovery of photosynthetic efficiency was measured during incubation at *in situ* temperatures and low light levels. In parallel experiments the repair of photodamage was prevented by addition of the inhibitor lincomycin. Lincomycin inhibits transcription of chloroplast encoded proteins, such as the D1 protein, which is a crucial component of photosystem II and one of the first proteins to become damaged by high light.

11.2 Preliminary data

In all experiments Fv/Fm was greatly reduced after incubating *in situ* phytoplankton samples in deck incubators at incident light levels for 20 min (see Fig 11.1 for typical examples from the SIZ and Ross Sea Polynya). This was observed in both samples from the surface as well as the chlorophyll maximum. Part of the decrease in photosynthetic efficiency was reversible during 120 mins of recovery under low light conditions. The inhibition of repair by the addition of lincomycin did not affect the initial decrease in photosynthetic efficiency, but reduced the recovery in most experiments, especially in the deep samples. These results indicate that photoinhibition affects phytoplankton photosynthesis in the SIZ, the Ross Sea polynya, as well as the ACC and thus protection from mechanisms such as photoprotective pigments and non-photochemical quenching do not completely prevent photodamage. Thus, repair of PSII is an

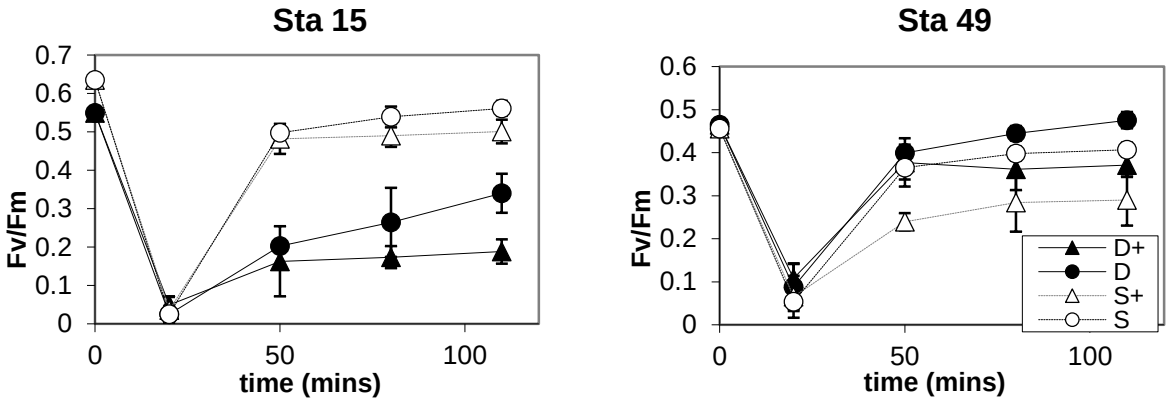

Figure 11.1. Examples for Fv/Fm responses after surface irradiance exposure for 20 min. Means and std of the Fv/Fm of triplicate cultures is shown before and after the exposure. Phytoplankton at Sta 15 in the sea ice zone (SIZ) north east of the Ross Sea showed a big difference in response between surface phytoplankton (S, open symbols) with very little slow recovery and subsurface phytoplankton (D, black symbols) with little fast recovery, mostly slow recovery, and a significant effect of blocking photodamage repair by the addition of lincomycin (triangles, D+). At Sta 49 in the Ross Sea Polynya there was little slow recovery after surface exposure of either surface or subsurface phytoplankton and lincomycin had a bigger effect in surface phytoplankton populations.

important mechanism to retain optimal photsynthesis rates for phytoplankton in the upper mixed layer. These results will be related to light levels in the upper mixed layer, exposure light levels, photoprotective vs photosynthetic pigment rates and phytoplankton species composition.

12. C:N:P Stoichiometry and Macromolecular Composition

Kate Lewis

Macromolecules in phytoplankton cells exhibit unique stoichiometric ratios: nitrogen (N) rich components include primarily proteins, phosphorus (P) components are mainly nucleic acids and polyphosphates, and carbon (C) is affected by carbohydrates and lipids[1,2]. Thus, phytoplankton cellular stoichiometry (C:N:P) is a reflection of its macromolecular composition, which phytoplankton adapt to achieve ideal growth strategies in given environmental conditions[3]. Previous research suggests that within the Ross Sea, spatially and taxonomically distinct annual phytoplankton blooms occur, which are primarily correlated with varying mixed layer depth (MLD) [4]. Previous measurements of nutrient disappearance ratios by Arrigo et al. (2000) indicate the two dominant bloom taxa exhibit unique N:P stoichiometries; Ross Sea diatoms typically have a lower N:P ratio (~12) than *Phaeocystis antarctica* (~19). Climate change threatens to dramatically shift the phytoplankton community structure towards diatom dominance by increasing stratification and thus causing shallower MLD. Because of the unique taxonomic differences in nutrient stoichiometry, shifts in phytoplankton dominance could have a large impact on regional biogeochemistry by decreasing the effectiveness of the biological pump (CO_2 drawdown and carbon export) by as much as 50%[4].

Macromolecular sampling on the NBP1310 cruise addresses two primary questions:

1. What is the cause at a macromolecular level for the difference in bulk C:N:P stoichiometry between diatoms and *P. Antarctica*?
2. How do phytoplankton adjust macromolecules pools to respond to different environmental factors (e.g. iron, light, mixed layer depth, stage of bloom etc.)?

At two depths at every station (depths correspond to those chosen for full sampling parameters including P vs. E), samples were taken for bulk C:N:P and macromolecules. Phytoplankton were collected by filtering seawater through 25mm Durapore 0.65 µm filters for DNA, RNA, protein, POP and Whatman glass-fiber (GF/F) 0.7 µm filters for carbohydrates and polyphosphate. Following filtration, filters were immediately frozen in liquid nitrogen and stored at -80˚C until future analysis to be completed at Stanford University. Bulk C:N:P will be determined by POC/N and POP. The contribution to each elemental pool by macromolecules will be determined by the relative composition of the major macromolecular contributors (DNA, RNA, protein, polyphosphate, and carbohydrate). These samples were taken at 95 different sampling depths from the conventional CTD resulting in a total of 570 filtered samples.

12.1 References

1. Elser, J.J., D. R. Dobberfuhl, N.A. MacKay and J.H. Schampel. Organism Size, Life History, and N:P Stoichiometry. *BioScience.* **46.9**, 674–684 (1996).
2. Falkowski, P G. "Rationalizing Elemental Ratios in Unicellular Algae." *European Journal of Phycology.* **36**, 3-6 (2000)
3. Geider, Richard, and Julie La Roche. "Redfield Revisited: Variability of C:N:P in Marine Microalgae and Its Biochemical Basis." *European Journal of Phycology.* **37.1**, 1-17 (2002).
4. Arrigo, K. R., G.R. DiTullio, R.B. Dunbar, D.H. Robinson, M. VanWoert, D.L. Wortheh, and M.P. Lizotte. Phytoplankton Taxonomic Variability in Nutrient Utilization and Primary Production in the Ross Sea. *J. Geophys. Res.* **105,** 8827–8846 (2000).

13. Hydrogen peroxide measurements

Tom Delmont and Anton F. Post (Not on board)

Hydrogen peroxide is a strongly oxidizing molecule ubiquitous in small amounts in the oceans due to its production by many microorganisms as a by-product of oxidative metabolism. Consequently, most organisms possess functional machinery (especially, catalase peroxidases) to reduce these deleterious molecules into inert water molecules. However, hydrogen peroxide is expected to be found in high quantities in Antarctica polynyas during phytoplankton bloom events due to an important biological activity coupled to oxygen saturation in the water column. Therefore, we decided to quantify the concentration of hydrogen peroxide in the Southern Ocean, and to link its production and reduction to abundance of *Phaeocystis antarctica* single cells and colonies. We quantified hydrogen peroxide concentration using an ORION microplate luminometer at different depths (surface to 400m depth) of the "daily stations" in the Ross Sea polynya and the ACC (464 samples). Moreover, we quantified hydrogen peroxide in the iron and light bioassay experiments (252 samples) to study the effect of Fe and light availability on its production and reduction.

13.1 Preliminary results

Interestingly, in the ACC, hydrogen peroxide concentrations were higher within the phytoplankton bloom relative to its surrounding environment, suggesting a relationship between high hydrogen peroxide

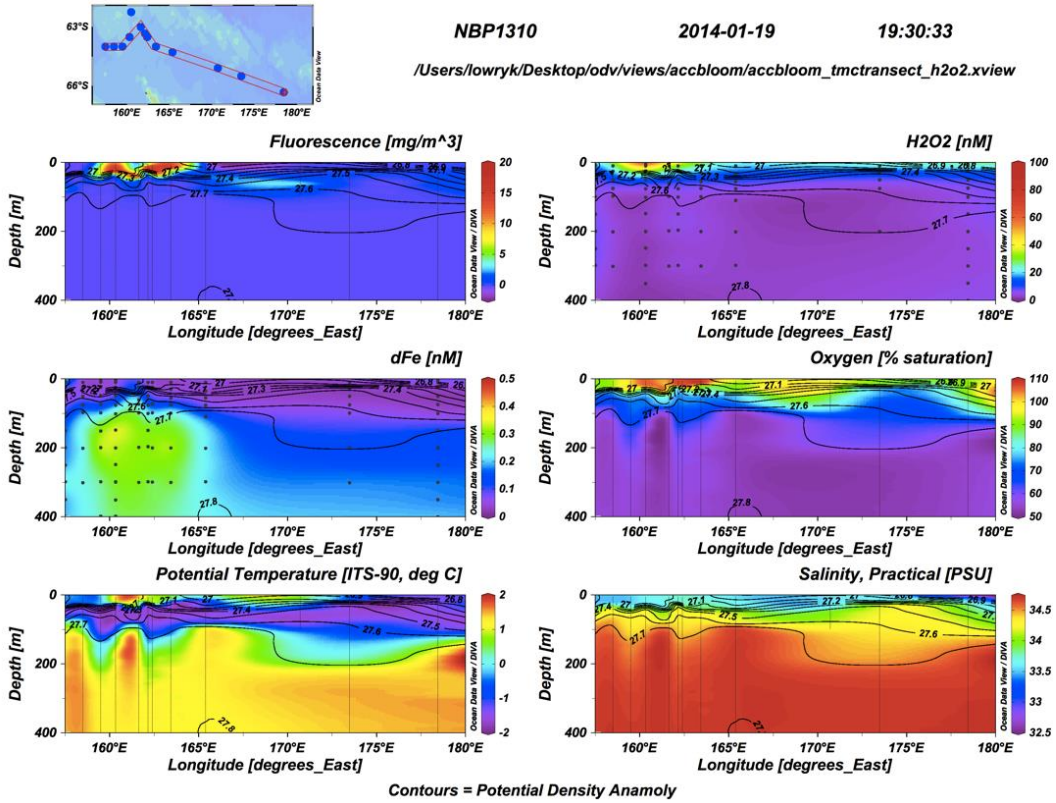

Figure 13.1. Depth profiles of fluorescence intensity, hydrogen peroxide (H_2O_2) and dissolved iron (dFe) concentrations, as well as oxygen saturation in 9 stations in the Antarctica Circumpolar Current. The phytoplankton bloom was observed between Longitude 158°E and 165°E.

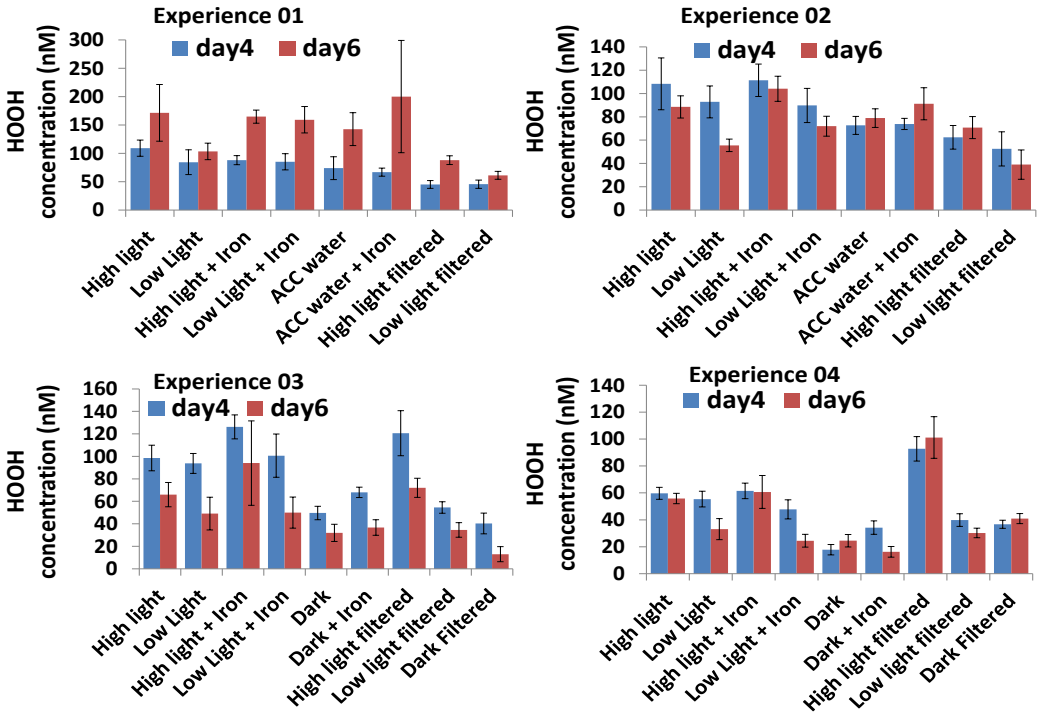

Figure 13.2 Hydrogen peroxide concentrations (error bars represent standard deviations) in 4 bottle experiments performed in the Ross Sea polynya. Each experimental condition was quantified using biological triplicates and technical duplicates. "ACC water" represents an experiment where Ross Sea polynya samples where diluted with water from the Antarctica circumpolar current. "Low light filtered" and "high light filtered" represent control conditions with filtered water. "Dark" represent conditions performed in complete dark.

concentrations and Chl fluorescence and oxygen saturation measurements (Fig 13.1). Furthermore, hydrogen peroxide concentration was quantified in the iron and light bioassay experiments performed in the Ross Sea (Fig 13.2) and Antarctica circumpolar current (data not shown). As expected, light increases resulted in an increase in hydrogen peroxide concentrations. But interestingly, iron additions resulted in most cases to a decrease in hydrogen peroxide concentrations, suggesting this element to help the phytoplankton reducing this oxidative molecule in spite of an increase in photosynthetic activity.

14. Satellite Remote Sensing

Gert van Dijken

Ocean color satellite images showing phytoplankton biomass distributions were paramount to the success of this cruise. Using these images as a guide, we were able to track areas with high phytoplankton biomass in our quest to sample *Phaeocystis* dominated waters in the Ross Sea. Also, through these images we 'discovered' the unusually intense phytoplankton bloom in the ACC area.

An automated system was set up at Stanford University to have MODIS/Aqua oceancolor data send to us on the research vessel by email. Through two near real-time data subscriptions using the NASA Ocean Biology Processing Group's data subscription service satellite scenes were downloaded every 3 hours from NASA ftp-servers. One subscription covered the Ross Sea and the other one the ACC area. After

downloading the files the chlorophyll product was extracted and mapped to a common projection. Daily composites were generated from individual scenes (4-8 per day) as well. In addition ice concentration data was downloaded from the National Snow & Ice Data Center (NSIDC) and reprojected the same way as the ocean color data. All images were then emailed to us in a compressed kml format (kmz), so it could be easily used with the Google Earth software package. See examples of these images elsewhere in the cruise report.

15. *Phaeocystis antarctica* proteomics

Miao Wu (not on board), Mats Sandgren (not on board), Tom Delmont, Bethany Jenkins, Anne-Carlijn Alderkamp

The main goal for this collaborative research project between Stanford University and the Swedish University of Agricultural Sciences (SLU) is to biochemically study key proteins in the metabolic pathways of *Phaeocystis antarctica*. Characterizing key metabolic proteins of *P. antarctica* will provide insights into the biochemical basis for this phytoplankton's success in adapting to the specific conditions of the Antarctic ecosystem. This goal will be achieved by utilizing a combination of bioinformatics, proteomics, molecular biology, biochemistry, and x-ray crystallography methods to study the proteins involved in nutrient acquisition and extracellular muco-polysaccharide production by *P. antarctica*, as well as to elucidate the effects of iron limitation and super-cooling on metabolic pathways.

15.1. Filtration of samples for Phaeocystis proteome analysis

At 38 stations phytoplankton biomass was collectedby filtering 2-36 L on filters that were stored at -80°C. To obtain enriched biomass for proteomic analysis, at Stations 112 and 114 in the Ross Sea Polynya that were dominated by *Phaeocystis antarctica*, either 12 or 22 Niskin bottles tripped at the chlorophyll maxima were drained over 105 µm mesh and then filtered onto 105 µm mesh cut in 47 mm circles and preserved at -80 ˚C.

To study effects of iron and light availability on protein expression in *P. antarctica* we sampled a complete set of extra bottles from bioassay experiments in the Ross Sea (experiments 1-4) and those in the ACC with high *Phaeocystis* biomass (experiments 7 & 8). Protein and backup RNA samples were collected onto 47 mm 3 µm filters and RNA volumes averaged 400 ml per filter and proteome volumes averaged 1700 ml collected onto 3 filters combined into one tube. Chl and nutrient samples were also taken from the bottles that were sampled for RNA and protein.

16. Macromolecular composition of *Phaeocystis antarctica* - Fourier Transport Infrared microspectroscopy and Raman spectroscopy

Olivia Sackett (not on board), John Beardall (not on board), Phil Heraud (not on board), Kate Lewis, Anne-Carlijn Alderkamp

16.1 Introduction

Each year, photosynthesis by marine phytoplankton converts ~58 petagrams (58 x 1015 grams) of atmospheric carbon dioxide into organic carbon molecules, equivalent in magnitude to terrestrial vegetation, creating half the oxygen we breathe as a by-product[1]. Southern Ocean phytoplankton constitute an important component of the global biogeochemical cycle, support the most biologically productive ecosystem on earth and constitute a significant net sink of atmospheric CO_2[2]. Phytoplankton in surface waters accumulate nutrients and trace metals, including N, P, Si, Fe, Mn, Ni, Cu and Zn, which can then be exported to depth as sinking biogenic particles or consumed by higher trophic levels[3]. Short-term physiological and metabolic adjustments in response to transitory changes in environmental conditions are

known as acclimation. Acclimation can result in substantial changes to the macromolecular composition of phytoplankton. Variations in the relative proportions of proteins, lipids and carbohydrates in microalgae may have dramatic implications for grazers. For example, as lipids contain ~2 and 2.3 times as many calories per unit biomass as proteins and carbohydrates (respectively), algal cells rich in lipids may contain more energy per unit biomass than those rich in proteins or carbohydrates[4]. Changes in the phenotypes of phytoplankton communities directly affect biogeochemical cycling in the ocean, as well as ecosystem structure and function[5].

The Southern Ocean ecosystem is profoundly affected by the seasonal duration and extent of winter sea ice. Changes to Sothern Ocean sea ice algae communities due to altered seasonal duration and extent of sea ice are likely to impact higher trophic levels since sea ice algae are a key component of the Antarctic food web[6,7]. Indeed, reduced duration and extent of winter sea ice along the West Antarctic Peninsula have been correlated with a decline in krill abundance and increased abundance of salps (a jellyfish-like planktonic organism) the following summer, however the mechanisms behind these trends are yet to be elucidated[8]. Laboratory studies have demonstrated that zooplankton growth rate and reproductive success can be directly affected by the growth phase and macromolecular composition of their phytoplankton food source[9,10]. In combination with observations from the West Antarctic Peninsula, these studies indicate that further examination of phytoplankton responses to environmental conditions and the flow-on effects to higher trophic levels is warranted.

Our previous beamtime at the Australian Synchrotron featured a study of diatoms sampled near the Kerguelen Islands in November 2011. Upwelling along the plateau and coastal areas provides naturally iron enriched waters which stimulate the largest bloom of phytoplankton south of the polar front[11]. Synchrotron Fourier Transport InfraRed (FTIR) microspectroscopy was used to analyze the macromolecular composition of individual diatom cells, generating the first known taxon-specific dataset of its kind. The study revealed taxon-specific phenotypic responses to iron availability and challenged the generally held view that iron limitation stimulates increased silicification in marine diatoms[12]. The current project will use FITR microspectroscopy and Raman spectroscopy to address several questions raised by the previous study including: How do other key phytoplankton species (i.e. *Phaeocystis* spp.) respond to iron availability? Do bulk elemental ratios reflect those of key phytoplankton species? How are elemental ratios related to nutritional value? This knowledge will help us predict how the Southern Ocean ecosystem and biogeochemical cycling may be affected by phytoplankton responses to climate change.

16.2 Aims

1. Characterise taxon-specific changes in macromolecular composition, elemental stoichiometry and cellular elemental quotas in response to iron and light-availability.
2. Characterise the relationship between iron-availability and silicon deposition in key phytoplankton taxon.
3. Identify which species may be more important for biogeochemical cycling of Si, Fe and P.

16.3 Sampling

Phytoplankton samples were collected from "daily stations" from the surface and chl maximum, form depths corresponding to the PE analysis (see section XX). In addition, samples were collected from the day 4 sampling from the Fe and light bioassay experiments (See section XX). Duplicate samples of six ml water was fixed with 1% formalin and stored at 4°C until analysis at Monash University.

16.4 References

[1] C. B. Field, M. J. Behrenfeld, J. Randerson, and P. Falkowski, Science (80-.)., 1998, 281, 237–240.
[2] A. J. Busalacchi, Antarct. Sci., 2004, 16, 363–368
[3] B. S. Twining, S. B. Baines, S. Vogt, and M. D. de Jonge, J. Eukaryot. Microbiol., 2008, 55, 151–162.
[4] J. N. C. Whyte, Aquaculture, 1987, 60, 231–241.
[5] Z. V Finkel, J. Beardall, K. J. Flynn, A. Quigg, T. A. V Rees, and J. A. Raven, J. Plankton Res., 2010, 32, 119–137.
[6] V. Smetacek and S. Nicol, Nature, 2005, 437, 362–368.

[7] A. McMinn, K. G. Ryan, P. J. Ralph, and A. Pankowski, Mar. Biol., 2007, 151, 985–995.
[8] A. Atkinson, V. Siegel, E. Pakhomov, and P. Rothery, Nature, 2004, 432, 100–103.
[9] J. D. Long and M. E. Hay, Limnol. Oceanogr., 2006, 51, 988–996.
[10] A. B. S. Diekmann, M. A. Peck, L. Holste, M. A. St John, and R. W. Campbell, J. Plankton Res., 2009, 31, 1391–1405.
[11] B. Queguiner, S. Blain, and T. Trull, The Kerguelen Plateau Proofs, 2007, 167–172.
[12] O. Sackett, J. Beardall, L. Armand, P. Ralph, and P. Heraud, Biogeosciences KEOPS2 Spec. Issue (in Prep., 2014.

17. Acoustic observations

Laughlin Barker and Benjamin L. Saenz (not on board)

During NBP13-10 cruise the otherwise would-be dormant acoustic echo sounder (Simrad EK60) was operated to collect acoustic information. The EK60 system aboard the N.B. Palmer utilizes 38, 120, and 200 kHz transducers. The 120 and 200 kHz transducers were activated and recorded data for the entire cruise when not in EEZs. The 38kHz transducer was operated during transits between oceanographic stations, and when the conventional CTD was being deployed. The intermittent use of the 38kHz transducer was due to fact that that one of the ADCP transducers also operates on 38kHz, and provides invaluable information regarding ocean currents and water mass transport.

The goal of operating the EK60 was to gain a better idea of the abundance and distribution of krill populations in the Ross Sea, specifically *Euphausia crystallorophias* and *Euphausia superba*. A group from NOAA has been performing acoustic krill surveys around Elephant Island and the Bransfield Strait for approximately 20 years aboard the N.B. Palmer, but relatively few investigations have looked into the abundance of these krill in the Ross Sea.

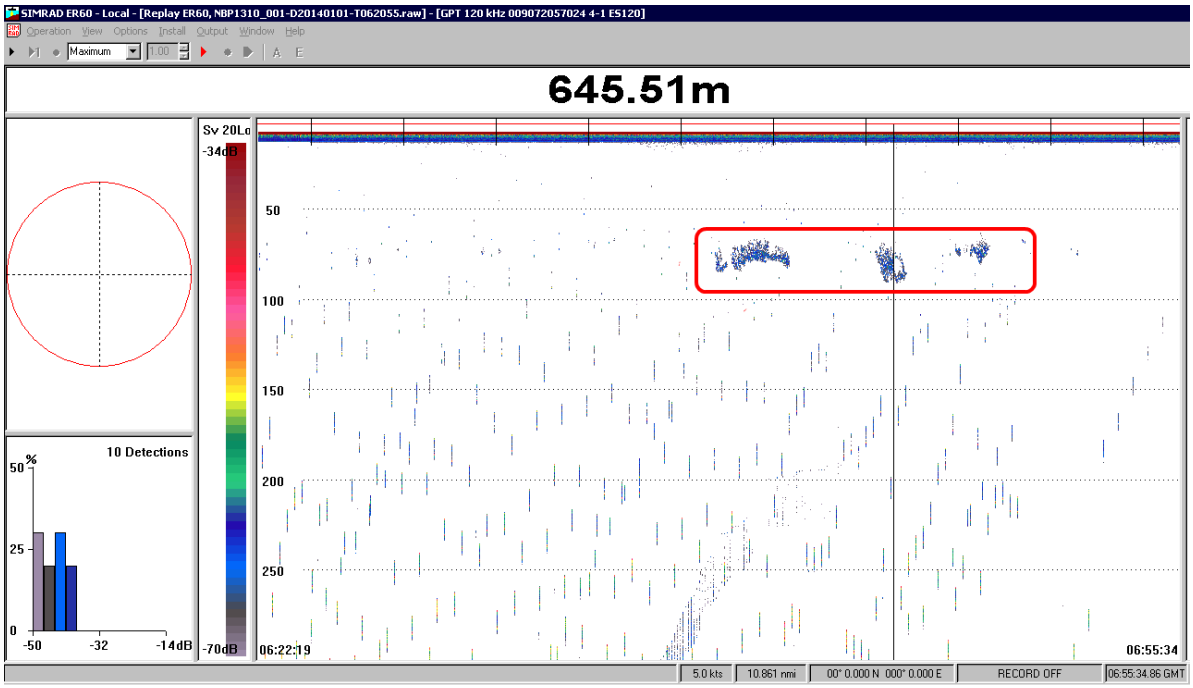

Preferential grazing by krill on certain phytoplankton could affect the population structure of the phytoplankton communities observed and studied during the cruise, and is thus of significant interest. Net-

Figure 17.1: A suspected krill bloom (red box) shown on the 120kHz echo sounder aboard the "N.B. Palmer" at a depth of approximately 80 m depth. Post processing will spatially integrate acoustic data to approximate size and biomass of the observed blooms.

tows are traditionally used to ground-truth the nature of a bloom seen on sonar, but were outside the scope of this project and were thus not performed.

Over fifty days of acoustic data were recorded, and will be post processed upon returning to the United States. Figure 17.1 shows a patch of suspected krill on the 120kHz transducer at a depth of 80m. Post processing will incorporate GPS data to spatially integrate the data to calculate approximate biomass and observed bloom length.

18. Argo Float deployments

A. Rick Rupan, University of Washington (not on board)

Argo is a broad-scale global array of temperature/salinity profiling floats that has grown to be a major component of the ocean observing system. It will provide a quantitative description of the changing state of the upper 2km of the ocean and the patterns of ocean climate variability from months to decades, including heat and freshwater storage and transport. A primary focus of Argo is to document seasonal to decadal climate variability and to aid our understanding of its predictability. A wide range of applications for high-quality global ocean analyses is anticipated. As of January 8, 2014 there are 3675 active floats. On the NBP 13-10, 21 Argo floats were deployed by the ASC marine technicians in and around the Ross Sea, which is an area that has not had any Argo deployments before.

Table 18.1 Argo float deployments

#	GMT Date (2013)	Latitude	Longitude	More information
1	11-Dec	64° 54.6 S	124° 00.0 W	http://runt.ocean.washington.edu/argo/homographs/TP/8498.html
2	11-Dec	64° 59.9 S	127° 59.7 W	http://runt.ocean.washington.edu/argo/homographs/TP/8461.html
3	12-Dec	65° 04.2 S	132° 00.0 W	http://runt.ocean.washington.edu/argo/homographs/TP/8464.html
4	12-Dec	65° 00.0 S	135° 52.1 W	http://runt.ocean.washington.edu/argo/homographs/TP/8458.html
5	13-Dec	65° 00.0 S	140° 00.2 W	http://runt.ocean.washington.edu/argo/homographs/TP/8467.html
6	13-Dec	64° 52.9 S	144° 00.7 W	http://runt.ocean.washington.edu/argo/homographs/TP/8795.html
7	14-Dec	65° 26.6 S	148° 00.0 W	http://runt.ocean.washington.edu/argo/homographs/TP/8820.html
8	15-Dec	66° 03.7 S	150° 00.0 W	http://runt.ocean.washington.edu/argo/homographs/TP/8487.html
9	15-Dec	66° 46.2 S	152° 00.5 W	http://runt.ocean.washington.edu/argo/homographs/TP/8789.html
10	15-Dec	67° 20.9 S	153° 56.4 W	http://runt.ocean.washington.edu/argo/homographs/TP/8477.html
11	19-Dec	74° 54.4 S	156° 00.0 W	http://runt.ocean.washington.edu/argo/homographs/TP/8409.html
12	20-Dec	75° 18.4 S	157° 59.9 W	http://runt.ocean.washington.edu/argo/homographs/TP/8480.html
13	20-Dec	76° 27.0 S	159° 59.6 W	http://runt.ocean.washington.edu/argo/homographs/TP/8451.html
14	20-Dec	77° 30.1 S	161° 59.9 W	http://runt.ocean.washington.edu/argo/homographs/TP/8401.html
15	20-Dec	77° 30.1 S	164° 00.0 W	http://runt.ocean.washington.edu/argo/homographs/TP/8495.html
16	21-Dec	77° 30.0 S	166° 00.0 W	http://runt.ocean.washington.edu/argo/homographs/TP/8483.html
17	21-Dec	77° 20.7 S	168° 00.4 W	http://runt.ocean.washington.edu/argo/homographs/TP/8450.html
18	21-Dec	77° 11.2 S	170° 00.0 W	http://runt.ocean.washington.edu/argo/homographs/TP/8809.html
19	21-Dec	77° 01.9 S	171° 59.9 W	http://runt.ocean.washington.edu/argo/homographs/TP/8472.html
20	21-Dec	76° 52.1 S	174° 00.0 W	http://runt.ocean.washington.edu/argo/homographs/TP/8823.html
21	21-Dec	76° 47.1 S	175° 00.2 W	http://runt.ocean.washington.edu/argo/homographs/TP/7670.html

19. Outreach

During this cruise, Dr. Bethany Jenkins maintained a blog (phantasticvoyage.wordpress.com) that was followed by her sister's AP biology class in Addison, IL, as well as students and faculty at the University of Rhode Island and Stanford. The blog featured scientist profiles as well as observations and descriptions of our project and scientific sampling. Jenkins and other scientists answered questions posted to the blog by students and the general public. The blog was highlighted on the University of Rhode Island's website and twitter feed.

Below selected content from the blog that showing the blog author (Jenkins' profile, a selected question from a high school student and response from chief scientist Alderkamp and Jenkins and the beginning of a scientist profile of Stanford PhD candidate s Kate Lowry written by Jenkins.

About

Welcome to Dr. Bethany's blog, where you can follow our 66-day research expedition from Punta Arenas, Chile to Hobart, Tasmania. Our research team is focused on single celled algae that live in the surface ocean. We are interested in how the metabolism of those algae are restricted by low iron concentrations in the Southern Ocean and the role light plays in these dynamics. We will be traveling to these really interesting areas that open up between the cold land and sea ice in the summer months. These open patches of water between the land and sea are called polynyas. They receive a lot of light and consequently are areas of intense growth of one of the groups of algae we are studying called Phaeocystis. Our name for our research cruise Phantastic derives from these organisms. Another group of algae that can also be very abundant in the Southern Ocean are diatoms, which are typically found in areas with slightly higher iron concentrations. These algae are characterized by their ability to bioprecipitate silicate to make glass shells. I'm interested in characterizing diatom communities and their nutrient metabolism in relation to the mosaic of light and nutrients in this part of the ocean.

Shivan Amn says: November 26, 2013 at 9:18 am

Hello Dr. Bethany,

I am a student in your sisters AP Biology class. In class we are currently learning about photosynthesis and how light effects the production of oxygen and sugar. The research you are conducting also deals with role light plays in algae, which i found really interesting. My question is that can excessive algae harm the fish and also can it harm the fresh water source?

Reply

phantasticvoyage says: November 27, 2013 at 10:48 am

From our chief scientist Dr. Anna:
Excessive algae can harm harm fish and fresh water sources in several ways. Some algae produce toxins that are actually poisonous for fish or shell fish that humans will eat, or for humans directly. In the 1960s there were reports penguins that died after consumption of krill that fed on one of the algae we are studying *Phaeocystis antarctica*. Also, if a lot of algae have grown and they die, bacteria start to decompose the algae and this can cause the water to become anoxic. That means the fishes can't breath anymore and it get's really stinky. Finally, if a lot of algae grow it can clog up pipes and pumps used for getting fresh water. Algae grow in both fresh water and seawater, so it is the same for both types of water.

And a comment from Dr. Bethany
Because Antarctica is so far from human development the growth of the algae down here are controlled by natural nutrient levels in the sea water. In regions close to where lots of humans live, sometimes too much nutrient inputs from things like sewage runoff and fertilizer runoff can cause too much algal growth making the problems Dr. Anna describes more severe.

DECEMBER 25, 2013

Scientist Profile: Kate Lowry

Kate Lowry is a biological oceanographer and PhD student in the laboratory of Dr. Kevin Arrigo at Stanford University. Kate's research combines both field intensive sampling with satellite oceanography to understand processes the control phytoplankton dynamics. She does

Appendix A

Table A1. List of stations with location (degrees North or East), date and time (GMT), CTD system (conventional or trace metal clean), bottom depth (m), cast depth (m), station type and area Rothera to Ross Sea (RtoR), Ross Sea, or Antarctic Circumpolar Current (ACC) area.

Station	Cast #	Latitude (S)	Longitude (E)	Date	Time	CTD System	Bottom Depth	Cast Depth	Station Type	Area
001	01	-65.697	-77.552	Dec 05	17:08	Conv	3991	401	Deep	RtoR
002	01	-65.000	-82.961	Dec 06	13:06	TMC	4524	401	Deep	RtoR
003	01	-64.999	-91.172	Dec 07	13:15	TMC	3553	401	Deep	RtoR
004	01	-64.999	-99.742	Dec 08	14:07	TMC	4888	401	Deep	RtoR
005	01	-65.000	-108.838	Dec 09	15:03	TMC	4945	402	Deep	RtoR
006	01	-65.000	-117.863	Dec 10	15:01	TMC	5568	402	Deep	RtoR
007	01	-65.001	-126.643	Dec 11	16:30	TMC	4883	401	Deep	RtoR
008	01	-65.001	-135.871	Dec 12	17:03	TMC	4690	400	Deep	RtoR
009	01	-64.872	-144.057	Dec 13	16:55	TMC	3796	402	Deep	RtoR
010	01	-65.448	-148.664	Dec 14	17:01	TMC	4157	400	Deep	RtoR
011	01	-67.349	-153.954	Dec 15	18:04	TMC	3697	401	Deep	RtoR
012	01	-69.678	-154.437	Dec 16	18:55	TMC	4772	401	Deep	RtoR
013	01	-71.619	-152.844	Dec 17	19:05	TMC	4329	400	Deep	RtoR
014	01	-73.365	-150.422	Dec 18	19:05	TMC	4140	400	Deep	RtoR
015	01	-75.017	-157.071	Dec 19	18:44	TMC	3687	1000	Deep	RtoR
	02	-75.026	-157.107	Dec 19	20:27	Conv	3687	101	Shallow	RtoR
016	01	-77.501	-162.001	Dec 20	18:55	TMC	650	625	Deep	Ross Sea
	02	-77.501	-162.001	Dec 20	20:25	Conv	650	111	Deep	Ross Sea
017	01	-77.500	-166.003	Dec 21	02:29	TMC	438	424	Deep	Ross Sea
	02	-77.500	-166.003	Dec 21	03:41	Conv	436	71	Shallow	Ross Sea
018	01	-76.501	-178.503	Dec 21	21:56	TMC	607	596	Deep	Ross Sea
	02	-76.501	-178.503	Dec 21	23:20	Conv	606	141	Shallow	Ross Sea
019	01	-76.501	177.495	Dec 22	05:25	Conv	373	101	Shallow	Ross Sea
020	01	-77.000	177.499	Dec 22	09:07	Conv	407	151	Shallow	Ross Sea
	02	-77.000	177.499	Dec 22	18:04	TMC	403	101	Exp 1	Ross Sea
	03	-76.999	177.512	Dec 22	19:30	TMC	405	51	Exp 1	Ross Sea
	04	-77.000	177.511	Dec 22	20:24	TMC	404	393	Deep	Ross Sea
	05	-77.001	177.512	Dec 22	21:37	Conv	404	91	Shallow	Ross Sea
021	01	-77.050	177.499	Dec 22	22:38	Conv	440	301	Butterfly	Ross Sea
022	01	-77.100	177.501	Dec 22	23:46	Conv	490	301	Butterfly	Ross Sea
023	01	-77.000	177.098	Dec 23	01:19	Conv	397	301	Butterfly	Ross Sea
024	01	-77.000	177.303	Dec 23	02:17	Conv	405	301	Butterfly	Ross Sea
025	01	-76.999	177.702	Dec 23	03:31	Conv	405	301	Butterfly	Ross Sea
026	01	-77.001	177.904	Dec 23	04:26	Conv	400	303	Butterfly	Ross Sea
027	01	-76.900	177.504	Dec 23	05:58	Conv	348	301	Butterfly	Ross Sea
028	01	-76.950	177.501	Dec 23	06:55	Conv	412	302	Butterfly	Ross Sea
029	01	-77.000	177.504	Dec 23	07:51	Conv	405	301	Butterfly	Ross Sea
030	01	-77.114	177.500	Dec 23	09:34	TMC	510	499	Iron	Ross Sea
031	01	-77.318	177.506	Dec 23	12:15	TMC	564	556	Iron	Ross Sea
032	01	-77.500	177.496	Dec 23	14:32	Conv	657	150	Shallow	Ross Sea
033	01	-77.317	177.500	Dec 23	18:23	TMC	586	101	Exp 2	Ross Sea

	02	-77.317	177.500	Dec 23	19:13	TMC	564	50	Exp 2	Ross Sea
	03	-77.317	177.500	Dec 23	19:45	Conv	564	300	Deep	Ross Sea
034	01	-77.367	177.499	Dec 23	20:59	Conv	598	301	Butterfly	Ross Sea
035	01	-77.417	177.499	Dec 23	22:11	Conv	633	301	Butterfly	Ross Sea
036	01	-77.317	177.104	Dec 23	23:38	Conv	569	301	Butterfly	Ross Sea
037	01	-77.317	177.297	Dec 24	00:29	Conv	568	301	Butterfly	Ross Sea
038	01	-77.316	177.698	Dec 24	01:36	Conv	576	300	Butterfly	Ross Sea
039	01	-77.317	177.893	Dec 24	02:24	Conv	592	300	Butterfly	Ross Sea
040	01	-77.217	177.501	Dec 24	03:56	Conv	542	301	Butterfly	Ross Sea
041	01	-77.267	177.500	Dec 24	04:50	Conv	550	301	Butterfly	Ross Sea
042	01	-77.317	177.498	Dec 24	05:48	Conv	565	301	Butterfly	Ross Sea
043	01	-77.500	177.500	Dec 24	07:51	TMC	684	671	Deep	Ross Sea
	02	-77.500	177.500	Dec 24	09:28	Conv	684	62	Shallow	Ross Sea
044	01	-77.737	177.540	Dec 24	12:11	TMC	753	743	Iron	Ross Sea
045	01	-77.666	177.508	Dec 24	14:22	TMC	742	732	Iron	Ross Sea
046	01	-76.750	177.500	Dec 24	21:38	TMC	295	287	Iron	Ross Sea
047	01	-76.500	177.497	Dec 25	00:23	TMC	373	363	Deep	Ross Sea
	02	-76.500	177.499	Dec 25	01:21	Conv	373	100	Shallow	Ross Sea
048	01	-76.000	177.499	Dec 25	20:22	TMC	449	440	Deep	Ross Sea
	02	-76.000	177.500	Dec 25	18:44	Conv	450	201	Shallow	Ross Sea
049	01	-75.500	177.504	Dec 26	00:59	TMC	426	410	Deep	Ross Sea
	02	-75.500	177.503	Dec 26	02:01	Conv	426	101	Shallow	Ross Sea
050	01	-75.549	177.502	Dec 26	03:11	Conv	428	351	Butterfly	Ross Sea
051	01	-75.601	177.501	Dec 26	04:10	Conv	434	351	Butterfly	Ross Sea
052	01	-75.500	177.103	Dec 26	05:58	Conv	410	351	Butterfly	Ross Sea
053	01	-75.500	177.300	Dec 26	06:58	Conv	418	375	Butterfly	Ross Sea
054	01	-75.500	177.702	Dec 26	08:20	Conv	438	351	Butterfly	Ross Sea
055	01	-75.501	177.902	Dec 26	09:23	Conv	424	351	Butterfly	Ross Sea
056	01	-75.400	177.499	Dec 26	11:05	Conv	401	351	Butterfly	Ross Sea
057	01	-75.450	177.500	Dec 26	12:12	Conv	422	351	Butterfly	Ross Sea
058	01	-75.499	177.496	Dec 26	13:12	Conv	426	351	Butterfly	Ross Sea
059	01	-75.000	177.501	Dec 26	18:12	TMC	368	356	Deep	Ross Sea
	02	-75.000	177.501	Dec 26	19:16	Conv	368	61	Shallow	Ross Sea
060	01	-74.500	177.500	Dec 27	18:17	TMC	273	265	Deep	Ross Sea
	02	-74.500	177.500	Dec 27	19:03	Conv	273	110	Shallow	Ross Sea
061	01	-74.433	176.500	Dec 27	21:33	TMC	297	289	Iron	Ross Sea
062	01	-74.417	176.099	Dec 28	00:19	TMC	416	406	Iron	Ross Sea
063	01	-74.383	175.701	Dec 28	03:09	TMC	490	480	Iron	Ross Sea
064	01	-74.367	175.234	Dec 28	05:56	TMC	532	505	Iron	Ross Sea
065	01	-74.333	174.500	Dec 28	18:10	TMC	551	535	Deep	Ross Sea
65	02	-74.333	174.501	Dec 28	19:14	Conv	551	450	Deep	Ross Sea
066	01	-74.383	174.500	Dec 28	20:26	Conv	540	440	Butterfly	Ross Sea
067	01	-74.433	174.501	Dec 28	21:28	Conv	541	460	Butterfly	Ross Sea
068	01	-74.333	174.102	Dec 28	23:13	Conv	570	491	Butterfly	Ross Sea
069	01	-74.334	174.297	Dec 29	00:23	Conv	553	470	Butterfly	Ross Sea
070	01	-74.333	174.699	Dec 29	01:49	Conv	544	460	Butterfly	Ross Sea
071	01	-74.334	174.902	Dec 29	02:56	Conv	539	460	Butterfly	Ross Sea
072	01	-74.234	174.500	Dec 29	04:49	Conv	574	495	Butterfly	Ross Sea

073	01	-74.284	174.501	Dec 29	05:55	Conv	557	476	Butterfly	Ross Sea
074	01	-74.334	174.501	Dec 29	07:02	Conv	554	476	Butterfly	Ross Sea
075	01	-74.500	172.500	Dec 29	18:05	TMC	528	517	Deep	Ross Sea
	02	-74.500	172.501	Dec 29	19:10	Conv	528	110	Shallow	Ross Sea
076	01	-74.550	172.501	Dec 29	20:22	Conv	526	447	Butterfly	Ross Sea
077	01	-74.600	172.500	Dec 29	21:27	Conv	527	447	Butterfly	Ross Sea
078	01	-74.499	172.125	Dec 29	23:13	Conv	507	426	Butterfly	Ross Sea
079	01	-74.499	172.309	Dec 30	00:15	Conv	516	436	Butterfly	Ross Sea
080	01	-74.501	172.684	Dec 30	01:37	Conv	535	456	Butterfly	Ross Sea
081	01	-74.500	172.872	Dec 30	02:44	Conv	512	431	Butterfly	Ross Sea
082	01	-74.400	172.499	Dec 30	04:23	Conv	518	437	Butterfly	Ross Sea
083	01	-74.450	172.501	Dec 30	05:27	Conv	514	435	Butterfly	Ross Sea
084	01	-74.500	172.501	Dec 30	06:30	Conv	530	451	Butterfly	Ross Sea
085	01	-75.000	172.001	Dec 30	17:56	TMC	542	532	Deep	Ross Sea
	02	-75.000	172.001	Dec 30	19:01	Conv	542	101	Shallow	Ross Sea
086	01	-75.499	170.999	Dec 31	00:36	TMC	564	554	Deep	Ross Sea
	02	-75.500	171.000	Dec 31	01:37	Conv	564	150	Shallow	Ross Sea
087	01	-76.000	170.001	Dec 31	18:06	TMC	621	611	Deep	Ross Sea
	02	-76.000	170.001	Dec 31	19:16	Conv	621	150	Shallow	Ross Sea
088	01	-76.110	168.750	Dec 31	23:01	TMC	440	430	Iron	Ross Sea
089	01	-76.098	168.880	Jan 01	00:58	TMC	487	475	Iron	Ross Sea
090	01	-76.083	169.041	Jan 01	03:10	TMC	527	517	Iron	Ross Sea
091	01	-77.000	171.000	Jan 01	17:59	TMC	735	151	Exp 3	Ross Sea
	02	-77.000	171.000	Jan 01	19:01	TMC	735	50	Exp 3	Ross Sea
	03	-77.000	171.000	Jan 01	19:26	Conv	735	655	Deep	Ross Sea
	04	-77.000	171.000	Jan 01	20:32	TMC	735	724	Deep	Ross Sea
092	01	-77.050	170.999	Jan 01	22:14	Conv	751	671	Butterfly	Ross Sea
093	01	-77.100	170.998	Jan 01	23:27	Conv	772	694	Butterfly	Ross Sea
094	01	-76.999	170.542	Jan 02	01:18	Conv	796	714	Butterfly	Ross Sea
095	01	-77.000	170.779	Jan 02	02:36	Conv	765	685	Butterfly	Ross Sea
096	01	-77.000	171.219	Jan 02	04:07	Conv	725	645	Butterfly	Ross Sea
097	01	-77.000	171.434	Jan 02	05:17	Conv	706	627	Butterfly	Ross Sea
098	01	-76.901	171.001	Jan 02	07:07	Conv	715	636	Butterfly	Ross Sea
099	01	-76.950	171.003	Jan 02	08:19	Conv	727	647	Butterfly	Ross Sea
100	01	-77.000	171.001	Jan 02	09:28	Conv	735	656	Butterfly	Ross Sea
101	01	-76.500	170.998	Jan 02	17:55	TMC	648	150	Exp 4	Ross Sea
	02	-76.500	171.000	Jan 02	18:55	TMC	649	50	Exp 4	Ross Sea
	03	-76.500	171.000	Jan 02	19:49	Conv	648	568	Deep	Ross Sea
101	04	-76.500	171.000	Jan 02	20:38	TMC	647	637	Deep	Ross Sea
102	01	-76.550	171.001	Jan 02	22:21	Conv	661	580	Butterfly	Ross Sea
103	01	-76.599	170.998	Jan 02	23:28	Conv	673	590	Butterfly	Ross Sea
104	01	-76.500	170.573	Jan 03	02:40	Conv	658	578	Butterfly	Ross Sea
105	01	-76.500	170.788	Jan 03	03:50	Conv	643	565	Butterfly	Ross Sea
106	01	-76.500	171.212	Jan 03	05:12	Conv	658	579	Butterfly	Ross Sea
107	01	-76.500	171.425	Jan 03	06:16	Conv	668	588	Butterfly	Ross Sea
108	01	-76.400	171.001	Jan 03	08:04	Conv	619	539	Butterfly	Ross Sea
109	01	-76.450	171.000	Jan 03	09:11	Conv	632	553	Butterfly	Ross Sea
110	01	-76.500	171.000	Jan 03	10:17	Conv	651	571	Butterfly	Ross Sea

111	01	-76.667	173.000	Jan 03	17:57	TMC	582	568	Deep	Ross Sea
	02	-76.667	173.000	Jan 03	19:05	Conv	582	110	Shallow	Ross Sea
112	01	-77.165	172.999	Jan 04	01:46	TMC	618	605	Deep	Ross Sea
	02	-77.166	173.000	Jan 04	02:58	Conv	618	200	Shallow	Ross Sea
112	03	-77.166	173.000	Jan 04	05:44	Conv	618	211	Shallow	Ross Sea
113	01	-77.233	175.000	Jan 04	17:59	TMC	435	423	Deep	Ross Sea
	02	-77.233	175.000	Jan 04	19:05	Conv	435	220	Shallow	Ross Sea
114	01	-77.332	177.489	Jan 05	01:38	TMC	576	564	Deep	Ross Sea
	02	-77.332	177.489	Jan 05	02:39	Conv	576	201	Shallow	Ross Sea
114	03	-77.332	177.489	Jan 05	04:49	Conv	576	250	Shallow	Ross Sea
	04	-77.332	177.489	Jan 05	06:40	Conv	575	250	Shallow	Ross Sea
115	01	-68.272	179.452	Jan 07	18:11	TMC	2969	401	Deep	ACC
	02	-68.266	179.474	Jan 07	19:09	Conv	2969	71	Shallow	ACC
116	01	-66.305	178.455	Jan 08	18:13	TMC	3752	401	Deep	ACC
	02	-66.305	178.455	Jan 08	19:09	Conv	3752	70	Shallow	ACC
117	01	-65.494	173.484	Jan 09	18:06	TMC	2700	402	Deep, exp 5	ACC
	02	-65.496	173.477	Jan 09	18:57	Conv	2700	51	Shallow	ACC
118	01	-65.087	170.711	Jan 10	03:05	TMC	3380	100	Shallow	ACC
119	01	-64.286	165.398	Jan 10	18:05	TMC	3099	401	Deep, exp 6	ACC
	02	-64.286	165.398	Jan 10	19:00	Conv	3103	51	Shallow	ACC
120	01	-63.987	163.447	Jan 11	03:45	TMC	3369	401	Deep, exp 7	ACC
	02	-63.987	163.447	Jan 11	04:36	Conv	3478	401	Deep	ACC
121	01	-63.988	163.560	Jan 11	06:04	Conv	3240	400	Butterfly	ACC
122	01	-63.988	163.674	Jan 11	07:07	Conv	3337	402	Butterfly	ACC
123	01	-63.888	163.446	Jan 11	08:47	Conv	3021	401	Butterfly	ACC
124	01	-63.938	163.447	Jan 11	09:46	Conv	3104	401	Butterfly	ACC
125	01	-64.038	163.446	Jan 11	11:16	Conv	3027	401	Butterfly	ACC
126	01	-64.088	163.445	Jan 11	12:23	Conv	2688	401	Butterfly	ACC
127	01	-63.988	163.217	Jan 11	13:59	Conv	3369	403	Butterfly	ACC
128	01	-63.988	163.331	Jan 11	15:02	Conv	3174	401	Butterfly	ACC
129	01	-63.987	163.448	Jan 11	16:10	Conv	3368	403	Butterfly	ACC
130	01	-63.500	162.400	Jan 11	21:12	Conv	2834	102	Shallow	ACC
	02	-63.500	162.400	Jan 11	21:34	TMC	2828	402	Deep, exp 8	ACC
	03	-63.499	162.400	Jan 11	22:22	Conv	2828	122	Shallow	ACC
131	01	-63.334	162.149	Jan 12	01:00	TMC	2899	502	Deep	ACC
	02	-63.334	162.149	Jan 12	02:00	Conv	2911	71	Shallow	ACC
132	01	-63.167	161.900	Jan 12	04:27	Conv	2888	403	Deep	ACC
133	01	-63.000	161.633	Jan 12	07:14	TMC	2858	403	Deep, exp 9	ACC
	02	-63.000	161.633	Jan 12	08:16	Conv	2865	402	Deep	ACC
134	01	-62.833	161.400	Jan 12	10:19	Conv	2903	400	Deep	ACC
135	01	-64.000	159.500	Jan 12	20:21	TMC	2762	401	Deep	ACC
	02	-64.000	159.500	Jan 12	21:14	Conv	2763	71	Shallow	ACC
136	01	-64.000	158.503	Jan 13	01:06	TMC	3000	401	Deep, exp 10	ACC
	02	-64.000	158.503	Jan 13	01:53	Conv	3091	121	Shallow	ACC

137	01	-64.000	158.833	Jan 13	03:52	Conv	2805	401	Deep	ACC
138	01	-64.000	159.167	Jan 13	05:29	Conv	2730	402	Deep	ACC
139	01	-64.000	159.832	Jan 13	08:00	Conv	2766	401	Deep	ACC
140	01	-64.000	157.500	Jan 13	18:06	TMC	3130	400	Deep	ACC
	02	-64.000	157.499	Jan 13	19:04	Conv	3130	401	Deep	ACC
141	01	-64.051	157.500	Jan 13	20:13	Conv	3203	401	Butterfly	ACC
142	01	-64.100	157.500	Jan 13	21:11	Conv	3264	400	Butterfly	ACC
143	01	-64.001	157.274	Jan 13	22:44	Conv	3263	401	Butterfly	ACC
144	01	-63.997	157.388	Jan 13	23:49	Conv	3240	401	Butterfly	ACC
145	01	-63.999	157.611	Jan 14	01:17	Conv	2499	400	Butterfly	ACC
146	01	-63.999	157.725	Jan 14	02:17	Conv	2702	401	Butterfly	ACC
147	01	-63.899	157.500	Jan 14	03:56	Conv	2480	400	Butterfly	ACC
148	01	-63.949	157.499	Jan 14	05:21	Conv	2827	401	Butterfly	ACC
149	01	-64.000	157.500	Jan 14	06:24	Conv	3126	400	Butterfly	ACC
	02	-64.000	157.500	Jan 14	08:00	TMC	3126	2001	Deep	ACC
150	01	-63.500	160.333	Jan 14	21:43	TMC	2786	407	Deep	ACC
	02	-63.500	160.334	Jan 14	22:44	Conv	2786	61	Shallow	ACC
150	03	-63.500	160.334	Jan 14	23:23	TMC	2789	2002	Deep	ACC
151	01	-63.500	162.408	Jan 15	07:51	TMC	2854	2002	Deep	ACC
152	01	-62.250	160.500	Jan 15	19:04	TMC	2585	1001	Deep	ACC
	02	-62.250	160.500	Jan 15	20:34	Conv	2585	101	Shallow	ACC

Appendix B- Cruise participants

Table B1. Cruise participants-Scientists

Name	Institute	Email address
onboard		
Anne-Carlijn Alderkamp	Stanford University	Alderkamp@Stanford.edu
Laughlin Barker	Moss Landing Marine Laboratories	Lbarker@mlml.calstate.edu Laughlinbarker@gmail.com
Tom Delmont	Marine Biological Laboratory (MBL)	Tdelmont@mbl.edu
Gert van Dijken	Stanford	Gertvd@stanford.edu
Loes Gerringa	Netherlands Institute for Sea Research (NIOZ)	Loes.gerringa@nioz.nl
Bethany Jenkins	University of Rhode Island	Bethany.Jenkins@gmail.com
Hannah Joy-Warren	Stanford	Hjoyw@stanford.edu
Patrick Laan	NIOZ	Patrick.laan@nioz.nl
Kate Lewis	Stanford	Kmlewis@stanford.edu
Kate Lowry	Stanford	Lowryk@stanford.edu
Casey Schine	Stanford	CMSmith9@Stanford.edu
Not onboard		
Kevin Arrigo	Stanford	Arrigo@stanford.edu
Hein de Baar	NIOZ	Hein.de.baar@nioz.nl
John Beardall	Monash University	John.eardall@monash.edu
John Dacey	Woods Hole Oceanographic Institution (WHOI)	Jdacey@whoi.edu
Phil Heraud	Monash University	Phil.heraud@monash.edu
Anton Post	MBL	Apost@mbl.edu
Rick Rupan	University of Washington	Rupan@ocean.washington.edu
Olivia Sackett	Monash University	Olivia.sackett@monash.edu
Benjamin Saenz	University of Colorado	Blsaenz@gmail.com
Mats Sandgren	Swedish University of Agricultural Science (SLU)	Mats.sandgren@slu.se
Philippe Tortell	University of British Columbia (UBC)	Ptortell@eos.ubc.ca
Leif Thomas	Stanford	Leift@Stanford.edu
Miao Wu	SLU	Miaowu81@hotmail.com

Table B2. Cruise participants-ASC

Name	**Position**
Alan Hickey	MPC
Richard Thompson	MT, lead
Matt Louis	MT
Matt Ulsh	MT
Tom Sigmund	MT
John R. Betz	MLT, lead
Gabrielle Inglis	ET, lead
Joe Tarnow	IT, lead
Bryan Chambers	IT